ABSTRACT

Title of thesis: EFFECTS OF FIRE WHIRL GENERATOR DIMENSIONS ON FLAME LENGTH AND BURNING RATE

Joseph Lee Dowling, Master of Science, 2020

Advisor: Professor Michael J. Gollner
Department of Fire Protection Engineering

In-situ burning remains an efficient method of oil spill cleanup, but the implementation of fire whirls over the spilled fuel has the potential increase the speed and efficacy of the process by increasing burning rate and temperature. Logistical requirements would then be placed on the size of the fire whirl generator. A range of wall heights between 0 and 55 cm were tested for a fixed-frame fire whirl generator with a liquid fuel source 10.5 cm in diameter to analyze the effect on the burning rate and flame length of resulting fire whirls. For very short walls, with heights approximately equal to the fuel pool diameter, an increase of almost double was shown in the mass loss rate. The flame length for the fire whirl increased drastically for wall heights above a critical value of 35 cm, forming stable on-source fire whirls. This indicates that the inflow boundary layer of the fire whirl is a crucial feature causing an increase in the burning rate, while a critical wall height is necessary for aerodynamic effects to form stable on-source fire whirls with extended flame lengths.

EFFECTS OF FIRE WHIRL GENERATOR DIMENSIONS ON FLAME LENGTH AND BURNING RATE

by

Joseph Lee Dowling

Dissertation submitted to the Faculty of the Graduate School of the
University of Maryland, College Park in partial fulfillment
of the requirements for the degree of
Master of Science
2020

Advisory Committee:
Professor Michael J. Gollner, Chair/Advisor
Professor Peter B. Sunderland
Dr. Sara McAllister

Acknowledgments

I would like to thank Dr. Michael Gollner, Dr. Sriram Hariharan, and Dr. Tao Xu for their guidance on the direction and data analysis for this project. I also wish to express my gratitude to Michael Jones and Anita Stoppel for their invaluable assistance with data collection.

I would like to acknowledge the Bureau of Safety and Environmental Enforcement (BSEE), U.S. Department of Interior, Washington, D.C. for funding early aspects of this work under contract No. E17PC00016. This work was primarily supported by the National Science Foundation (NSF, CBET-1507623).

Contents

Chapter 1: Introduction

1.1 Impact of Fire Whirls

Fire whirls have been known to occur in wildland and large urban fires with devastating consequences [1]. The interaction of buoyant fire plumes with wind blowing over surrounding topography can produce fire whirls, with ridges on surrounding terrain creating the ambient vorticity needed for fire whirl formation [2]. In urban settings, crossflow over an urban conflagration can produce deadly fire whirls like the one that ravaged the Hifukusho-ato area after the Great Kanto Earthquake of 1921 [3]. In the laboratory, sidewalls and vanes are often used to channel entrainment utilizing a fire's buoyancy as the driving mechanism of fire whirl formation. Research has shown there are many ways in which the necessary vorticity can be introduced to generate fire whirls, both in the laboratory and the field, with fire whirls exhibiting an intensification of combustion with higher fuel burning rates, longer flame lengths, and higher temperatures [4]. These observations recently motivated the study of fire whirls in the application of fuel spill cleanup, which is further explored here [5], [6].

1.2 *In-Situ* Burning

While it would be ideal to remove all spilled hydrocarbons after an accident, it is often very difficult to fully collect and dispose of oil or other liquid pollutants over open water.

Crude oil in particular emulsifies with water over time, giving a narrow window for efficient fuel cleanup. *In situ* burning is an alternative that can remove as much as 90% of a spill volume for sufficiently thick oil spills, converting that mass to atmospheric effluents. The method, however, produces potentially hazardous quantities of smoke proximal to the burn site, potentially endangering workers and nearby populations [7].

As stated earlier, fire whirls are known to have higher burning rates and temperatures compared to pool fires of comparable size and fuel type [5], [8]. These qualities would be beneficial to the burning of oil spills, as higher temperatures are beneficial for burning emulsified oil, and higher burning rates would reduce the duration of the burn [7]. Qualitatively, the effectiveness of fire whirls to burn liquid fuels over a water layer was shown by a fire whirl that formed over the surface of a Kentucky pond when a layer of liquor on the pond surface caught fire [9]. The generation of a fire whirl during an *in-situ* burn could be useful in producing cleaner and faster removal of the spilled fuel than a traditional *in-situ* burn. This was observed during recent testing from 10 to 70 cm diameter pool fires and fire whirls which showed decreases of up to 50% in the amount of particulate matter emissions at the largest tested scale [6]. This reduction in emissions may reduce the safety hazard that plumes from *in-situ* burning present.

If fire whirls are to be induced over open-water oil spills, then the dimensions of the generator used would be limited by the logistics of a floating structure, the availability to transport the generator, and the equipment needed to deploy and operate it. These logistical concerns would place demands on the size and operational design of a fire whirl generator. While there are many laboratory studies of fixed-frame fire whirl generators, none investigate the height of the apparatus necessary to induce fire whirl formation. This investigation, therefore focuses on the effects of the generator dimensions on fire whirl formation, flame height, burning rate, etc. for fixed-frame fire whirl generators.

In the experiments presented here, this was accomplished with a four-walled enclosure

with tangential gaps through which ambient air could be entrained.

Chapter 2: Literature Review

2.1 *In-Situ* Burning

In-situ burning of oil spills constitutes a near classic pool fire configuration. Liquid pool fires are a case of combustion where the burning area is fixed, and the burning rate is dominated by the evaporation of the liquid fuel into a combustible gas [10]. Radiant and convective heat transfer from the flame above increases the rate of fuel evaporation, causing an increase in burning rate and flame length [7]. As pool fires increase in size the mode of heat transfer often changes as does their burning efficiency, in part due to a lack of oxygen reaching the center of the burning region [6] .

2.2 Fire Whirl Generation

Fire whirls can form over any flame that has ambient vorticity and a fluid sink [8], [11]. Like a pool fire, a fire whirl is a non-premixed flame with a fuel rich interior in an external environment of ambient oxidizer [12]. The flame sheet forms when the concentrations of fuel and oxidizer are sufficient for combustion to propagate, while diffusion pulls more fuel and oxidizer into the reacting region to continue the combustion reaction. When tangential momentum is applied, referred to as swirl, to the pool fire, the rising buoyant plume provides the fluid sink necessary for the formation of the fire whirl vortex [4]. The bottom boundary layer of the fire whirl creates an inflow that drives the combustion of the fire

whirl via transport of evaporated fuel into the body of the flame [4], [13]. Fire whirls can form either on-source, where they are located over the fuel source, or off-source where the circulation concentrates in an area distant from the fuel source [14] . Fire whirl generators vary between open structure, which rely on topography, ambient wind, or fire arrays to generate circulation, and enclosed structures, which induce circulation by using obstructions to impose direction on entrained air [4]. Emmons-type fire whirl generators, as used in the pioneering work by Emmons and Ying [8], rely on a spinning mesh to induce circulation in the ambient air. A fixed-frame fire whirl generator is a subset of solid enclosure fire whirl generators that have been studied extensively in previous work due their ability to create a reproducible, quasi-steady, on-source fire whirl [4], [15]. Generators of this type induce a fire whirl by limiting air entrainment to velocities tangential to the fire source, creating a vortex over a centered fuel pool [4]. In a fixed-frame fire whirl generator, the entrained air produces a tangential velocity larger than the radial inflow velocity and increases the inflow to the burning region of the pool compared to a pool fire without swirl [16].

In an on-source fire whirl where the fuel pool surface is flush or close to flush with the bottom of the enclosure, the bottom boundary layer of a fire whirl can be described as an Ekman-like boundary layer due to the swirl over the fuel surface [13]. In an Ekman layer, the Coriolis force, frictional force of drag from the lower boundary, and the pressure gradient across the rotating fluid body balance by generating a net flow into the rotating body [17].

2.3 Fire Whirl Characteristics

The characteristics that make fire whirls exceedingly dangerous in wildland fires also indicate how useful they may be at removing a fuel from a surface. Compared to a non-whirling pool fire, the flame length can increase by factors exceeding 10 [4]. This increase

in flame height is due to the interaction of the circulation on the flow structure of the whirl as well as the increase to the burning rate [3]. The structure of a fire whirl can be described as a Rankine type vortex, with a rotational vortex core surrounded by an irrotational vortex [18]. Chuah et al. [19] model the fire whirl as a Burgers vortex with the buoyant flow providing the axial velocity needed to concentrate vorticity, and therefore the diameter of the vortex core becomes an important parameter, though Hayashi et al. in [20] argue that the Burke-Schumann-Burgers model employed by Chuah doesn't match experimental results. For a cylindrical fire whirl, the radius of the vortex core has a lower bound at the flame sheet [21], but is shown to exceed the flame radius by a large margin [16]. The Burke-Schumann-Burgers model can be seen in Figure 2.1, which shows the boundary layer flow of the azimuthal velocity at the edge and Burger's vortex model of azimuthal and axial velocity at the center, as well as an increased radial inflow at the bottom boundary.

The circulation of the vortex creates an Ekman-like boundary layer where the circulating air is slowed by drag from the boundary with the enclosure floor, creating a pressure difference that drives flow inward towards the axis of rotation in the boundary layer [22].

Li et. al. [13] identify three flow regions in the fire whirl: an Ekman-like inflow layer that entrains air, a whirling Burgers vortex in which the evaporated fuel is burnt, and a transition zone directly above the fuel pool that connects these regions. The resulting height of the flame correlates with how close this thin flame layer comes to the fuel surface [20], [23]. Within the bottom inflow layer, Lei et al. [24] further divide the surface of the fuel source into two regions, an outer region in which the evaporated fuel burns in the inflow layer, and an inner nonreactive region where the fuel evaporates but is transported higher into the flame to burn. This outer burning region experiences enhanced combustion due to the increased air entrainment from the inflow layer increasing local mixing [11]. The inner region is similar to the fuel-rich core of a Burke-Schumann flame [25], but it is stretched by the presence of swirl.

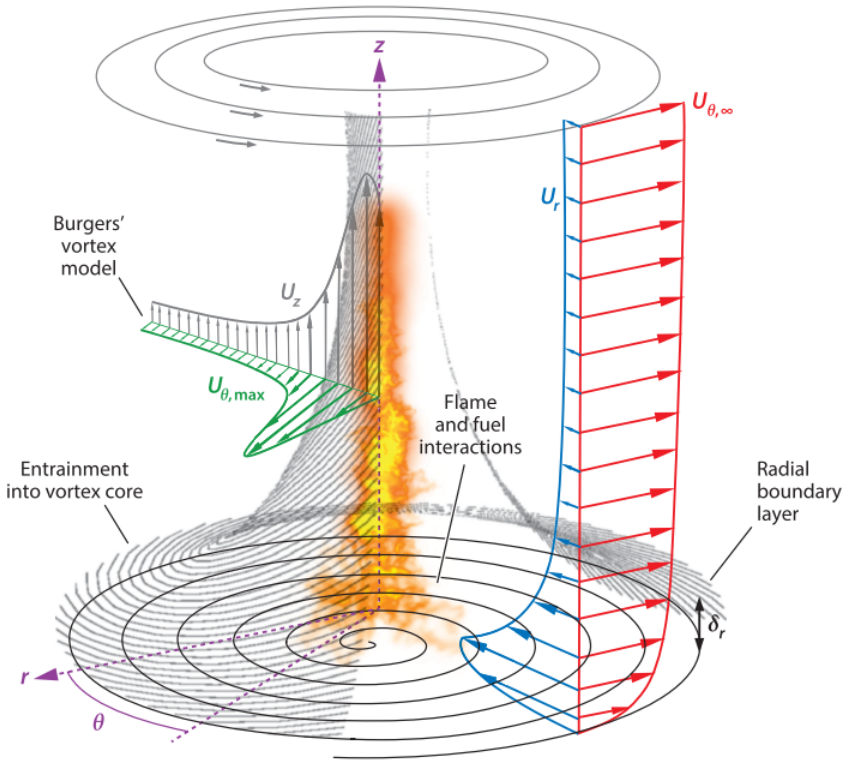

Figure 2.1: Depiction of the flows inside a fire whirl from Tohidi et al. [4]. Shown are the velocity profiles for the azimuthal, radial, and axial flows corresponding to a Burgers vortex model of the fire whirl.

Turbulent suppression of mixing accounts for some of the increase in flame length [4]. The circulation, induced or imposed, impedes the mixing of the ambient air along the length of the vortex core, increasing the visible burning length [15]. This would modify the effective diffusion coefficient in an application of Roper's equation for the height of diffusion flames, though Chuah and Kushida [21] treat the effect of swirl on diffusion as an effect on the vortex core radius. The other effect increasing the flame height is the action of vortex stretching, which, due to the conservation of angular momentum, reduces the radius of the vortex and increases its length [26].

The effect of circulation to increase the flame height does not persist for all values of circulation, as beyond a critical threshold, increasing circulation can cause flame detachment, and a decrease in flame height and burning rate [27]. Additionally, according to Lei, Liu, and Jiao [28] the effect of imposed circulation also depends on the heat release rate of the fire, as excessive circulation imposed over relatively weak fire whirls can cause irregular, flickering flame as well as extinction.

2.4 Scaling Fire Whirls

As realistic fire whirls are often too large and dangerous to reproduce in the laboratory, scaling the features of these fire whirls at reduced scale is a common experimental technique for their study [3].

2.4.1 Flame Height

The height of a fire whirl is dependent on both the buoyant action of the fire plume and the effect of the circulating flow, creating separate methods of scaling dependent on the relative strength of these effects. The difference in these regimes could be represented as

critical values of the Rossby number, which Tohidi et al. [4] define as

$$Ro = \frac{U_z H}{\Gamma} \tag{2.1}$$

with U_z as the axial velocity, H is the flame height, and Γ is the circulation. Emmons and Ying [8] also relied on the inverse of the Rossby number to define the formation of the fire whirl. If the inverse of the Rossby number can be considered comparable to the swirl number [4], then it could represent the ratio of axial to azimuthal momentum, such that low Rossby numbers describe a circulation-controlled fire whirl.

For a weak fire whirl, one where the buoyant action of the plume is dominant, the lengthening of the flame can be attributed to increased burning rate due to heat feedback to the fuel surface. The Ekman boundary layer pulls the flame sheet closer to the fuel surface, increasing the fuel heating and subsequently the rate of fuel evaporation [22]. The boundary layer inflow also increases the rate of convective mass transfer from the fuel surface [24]. The scaling of the flame height for these fire whirls relies on a nondimensional heat release rate that is comparable to the Froude number or Péclet number [22], [29]. Kuwana et al., for all weak fire whirls scale the dimensionless flame height linearly with the Péclet number [23].

For a circulation controlled regime, the increase in flame height can be attributed to the aerodynamic effect of vortex stretching and the limiting of turbulent mixing, which increases the length of the fuel rich vortex core [21]. In the case of an on-source fire whirl over a burner, the burning rate is decoupled from the flame geometry, so the circulation is the only controlling factor of height leading to a relationship defined by Hartl and Smits [30] as

$$H^* = 0.74\Gamma^{*1.11} \tag{2.2}$$

Increased circulation created by altering the angle of incidence from entrained air also produces a stretching effect on the flame length by changing the ratio of tangential to radial velocity [27]. Simulations of fixed frame fire-whirls posit that the hydrodynamic affect is the dominating factor in fixed-frame fire whirl generators with symmetrical wall gaps [31]

2.4.2 Burning Rate

The increased burning rate of a fire whirl compared to a pool fire suggests an influence of increased heat feedback to the surface of the fuel [4]. This increase in burning rate is dependent upon the boundary layer conditions, as shown by Dobashi et al. [22] in an experiment where the fuel surface was not contiguous with the enclosure floor; the discontinuity between the fuel surface and lower boundary of the enclosure prevented the creation of an Ekman-like boundary over the fuel and the experiment showed no increase in burning rate. Snegriev et. al. [11] show a slight decrease in radiative heat transfer to the fuel surface in fire whirls compared to normal pool fires, suggesting the decrease is due to a comparatively thinner flame than a pool fire and indicating a different mechanism of increased heat feedback. Lei et. al. [24] explain the enhancement of the burning rate effect as an increase in the convective heat and mass transfer, as the increase in burning rate is shown to be dependent on circulation even assuming a negligible contribution of radiation feedback from the flame sheet close to the fuel surface. In a circulation controlled regime, the burning rate correlates with the radial inflow speed generated in the boundary layer [19].

2.5 Flame Lengthening Effects from Generator Wall Height

The height of the enclosure wall may affect the formation of the fire whirl due to an influence on the boundary inflow layer as a result of the stack effect, or by increasing the axial region in which induced circulation remains sufficient to suppress turbulent mixing.

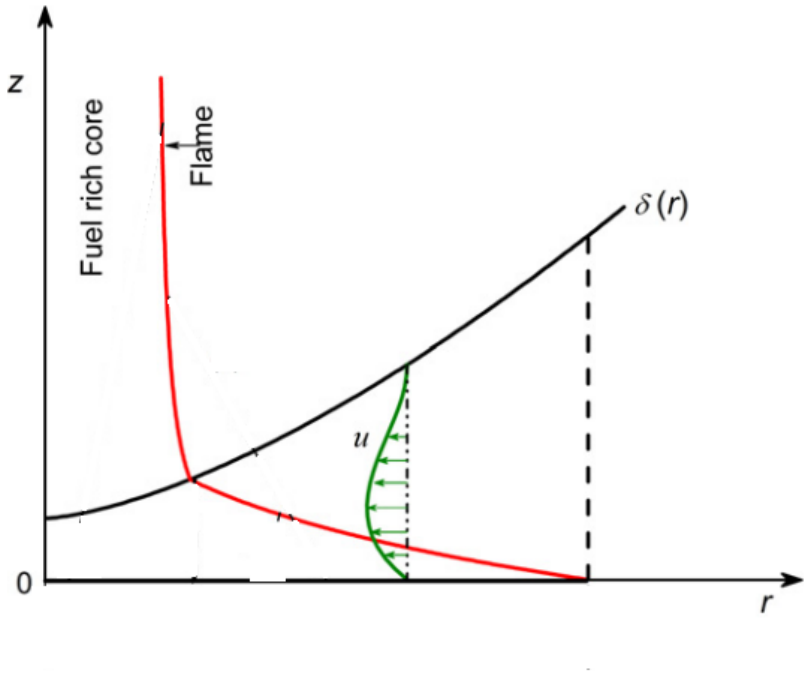

Figure 2.2: Depiction of the boundary layer inflow of the fire whirl from Lei et al. [24]. Shown are the radial inflow of the boundary layer, as well as the flame sheet and fuel rich region of the fire whirl

The stack effect refers to the induced inflow and outflow caused by a difference in density between gases inside and outside of an enclosure, such as the fixed-frame generator itself. At some point along the height of the enclosure, the pressure in the enclosure will equal the ambient pressure; this point may be referred to as the neutral plane. As the gases inside the generator are hotter and less dense than ambient air, the buoyant plume will draw the hot gases out of the top of the generator and cooler ambient air will fill the generator from the bottom. As the velocity with which the gases enter an enclosure varies as the square root of the vertical distance between the height of the opening and the height of the neutral plane [32], the increase in wall height may increase the velocity of the inflowing air by increasing the height of the neutral plane. In the pioneering investigation on fire whirls by Emmons and Ying [8], it was concluded that the turbulent mixing coefficient decreased with angular

momentum, but increased along the height of the plume. The force balance between the centrifugal force and the pressure gradient, as well as the stratification of the hot gases by density due to the centrifugal force, limit the ability for the gases to mix radially [4], [12]. This limits the effective entrainment of air along the length of the vortex, with a decrease in the entrainment coefficient as the ratio of tangential to axial velocity increases [12]. Figure 2.2 shows the higher velocity inflow into the fire whirl in the boundary layer, and shows the boundary layer growing with radial distance. Since the velocity profile entering a fixed-frame fire whirl generator shows a near-flat region at the bottom of the inlet gap with a high relative velocity [12], [31], one may expect that an increase in the height of the wall could increase the length of this region and extend the region in which turbulent mixing is effectively suppressed.

Chapter 3: Experimental Methods

3.1 Experimental Setup

The experimental setup consists of a fixed-frame type fire whirl generator with a square base and four walls surrounding a pool fire. A fuel dish (outer diameter 11.5 cm, inner diameter 10.5 cm) with a depth of 5.1 cm was filled with 430 mL of water, leaving room for 20 mL of n-heptane to be added as fuel, such that a fuel layer approximately 2.5 mm in depth is flush with the lip of the fuel dish. A 40 cm by 40 cm aluminum plate with a 12 cm diameter hole in the center was placed so that the top of the plate was flush with the lip of the pan and the fuel surface to prevent disruptions in the boundary layer of the entrained air. The fuel dish was supported by a load cell to record the time-dependent mass of remaining fuel, while the base plate was supported by a separate stand to prevent vibrations from affecting the load cell measurements.

Figure 3.1 shows a schematic of the fire whirl generator from an isometric view. As can be seen on this figre, the walls of the fire whirl generator were mounted to a frame that was not attached to the enclosure base. The enclosure base consisted of the metal base plate that was kept flush to the fuel surface, and the load cell that measured the fuel mass. The frame was constructed of slotted aluminum framing and affixed to sliding mounts to provide two degrees of freedom for each wall. The entire frame could be raised or lowered to change the effective height of the wall over the fuel layer, and each wall could be moved left or right to create a gap between the walls of variable width through which air entrainment could

be restricted. The panels were 60 cm high by 45.7 cm wide, and allowed for a maximum effective wall height of 55 cm above the fuel due to mounting hardware occupying the bottom 5 cm of the plates, and a minimum wall height of 30 cm above the fuel surface. A second set of plates, 30 cm high by 45.7 cm wide were constructed and used for testing with wall heights below 30 cm. One wall of each height was replaced with a clear polymethyl methacrylate (PMMA) sheet with the same dimensions to allow for video recording of the flame, and the base plate and back wall of the enclosure were painted matte black to reduce glare in the video.

The original design for the walled enclosure was similar to this final design. Both had affixed the walls to a horizontal carriage to increase or decrease the gap size and a vertical carriage to increase or decrease the wall height relative to the fuel dish. The original design also allowed for aperture motion of the walls to allow for different dimensions of the base plate. This necessitated that the walls be affixed only at the bottom. This extra degree of freedom and location of mechanical joints lead to vibrations during testing that influenced the mass loss data collection, and the setup had to be redesigned to avoid vibration by reinforcing the horizontal carriage and abandoning the interchangeability of the base plate. The original base plate was made of ceramic fiberboard, sealed with high temperature paint.

An HD video camcorder was mounted on a tripod and placed such that the bottom of the field of view of the camera was flush with the fuel surface and encompassed at least 60 cm of vertical space above the fuel dish. An AND load cell ($\pm$0.1 g) read the mass of the sample at a rate of approximately 1.75 Hz. A thermocouple was used to record the temperature of the surface of the water layer before the addition of fuel and was removed prior to testing. The water was replaced if it was beyond 35°C at the point before the addition of fuel or after the completion of three tests. At the end of each test, a meterstick was placed vertically over the center of the fuel dish to provide a reference image for the footage of the flame.

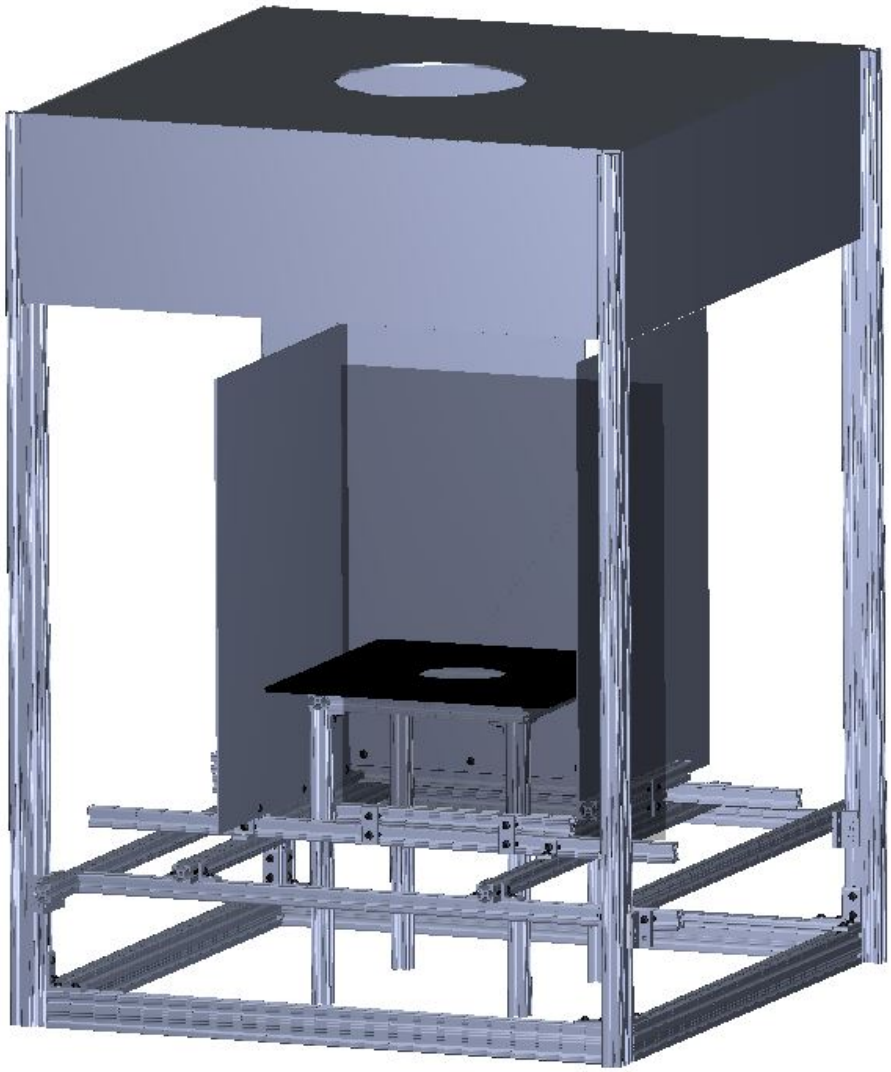

Figure 3.1: Isometric view of experimental setup, model courtesy of A. Stoppel

For tests with relative wall heights less than 40 cm (W $\leq$ 40 cm), the setup was placed underneath an exhaust system to vent the smoke from the testing laboratory. The exhaust inlet was 60 cm from the fuel surface and had a maximum inlet velocity of 9 m/s. At a relative wall height of 40 cm, the suction from the exhaust began to pull air through the base of the setup rather than from above the setup, causing inaccuracies in the mass loss data due to vibration and air flow over the load cell. The less than 1 mm gap between the fuel dish and the base of the enclosure created instances of high velocity air pulled through this gap by overhead suction, obfuscating the test results by applying extraneous forces to the load cell. Future tests with this wall height and all higher walls were conducted in a larger room where the smoke would not be evacuated by overhead suction during the test duration but could be vented at test completion.

3.2 Image Analysis Methods

For each filmed test, the video of the test was converted from AVCHD (Advanced Video Coding High Definition) to an MP4 format that could be read by Matlab. Each frame frame of the video was converted to black and white and then to 2-D matrix of brightness values. Due to the orientation of the camera during filming, the tip of the flame extended to left (the negative x direction) when so converted. For each column of pixels, which run perpendicular to the flame length, each pixel down the column was evaluated for brightness beyond a set threshold value. The first value in each column beyond this threshold was recorded, as well as the last value above this threshold. When this was done for each column the width and location of the flame would be known at each pixel along the x axis, allowing for the outline of the flame to be traced for each frame of video. A sample image is shown for pool fires in Figure 3.2 and for a fire whirl in Figure 3.3. The pixels in a 7 by 7 square surrounding that pixel were then evaluated for a brightness value beyond

the same threshold, as artifacting from the file conversion and deinterlacing produced dark stripes of a single pixel in width and the largest reflections of the flame from the setup were smaller than 7 by 7 pixels. The chosen threshold brightness was 254 as the camcorder was overexposed by the bright flame on the matte black backdrop.

The reference frame of each video was used to convert pixel lengths to centimeters, applied after each video was processed. The images provide flame length as a primary output, but also allow for the monitoring of the flame's precession about the fuel dish, as well as monitoring the effect of the entrained air to tilt the flame away from perpendicular toward the base. The width of the flame could then be averaged along the flame length for each flame to produce a horizontal length scale for use in analysis. One of the shortcomings of the primitive computer-vision techniques that were used is the inability for the width of the flame to be resolved into multiple flame structures. This is relevant in the unsteady periods before the fire whirl forms and stabilizes, as the flame occasionally formed additional tongues while flickering.

3.3 Velocity Measurements

Hot-wire anemometers were positioned along the centerline of one gap on the generator to measure the velocity of the entrained air perpendicular to the gap. A configuration with a 55 cm effective wall height was used as a representative fire whirl case, whereas a wall height of 15 cm was used as a representative pool fire case. A gap size of 10.5 cm was used in both cases. Anemometers were positioned at heights of 0.5, 2.5, 5, and 45 cm above the base plate for the fire whirl case,and at 2.5 and 5 cm above the base plate for the pool fire case. Air velocity data was logged with a frequency of 0.5 Hz

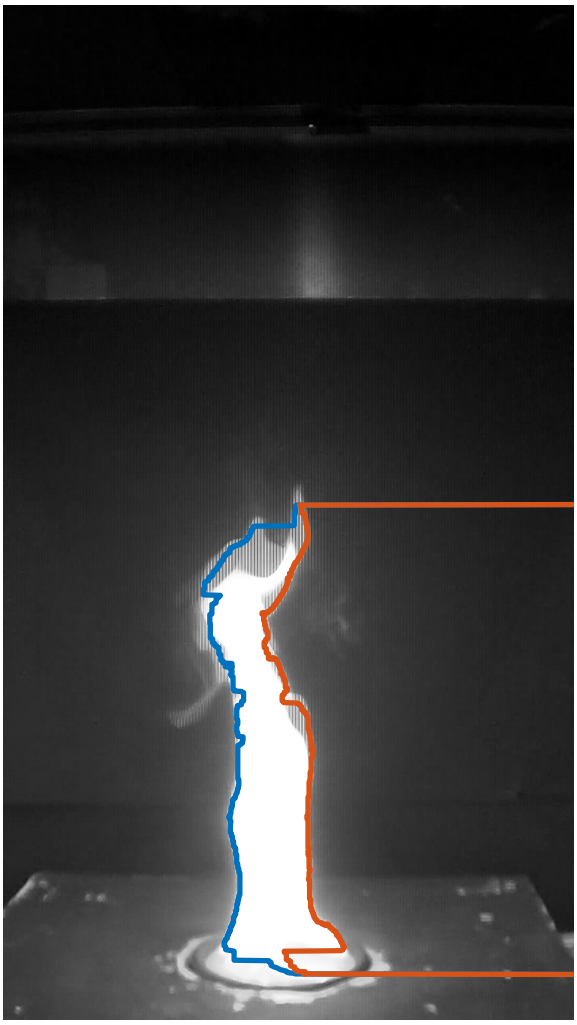

Figure 3.2: Analysis of Sample Pool Fire Frame, Outline shown in orange and blue show the right and left edges of the flame for the intents of image analysis calculations

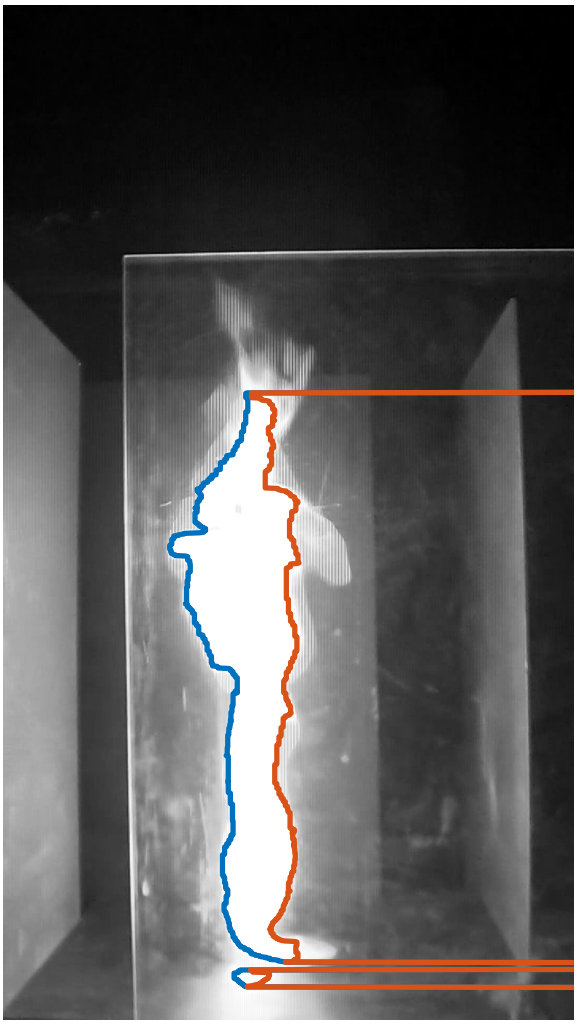

Figure 3.3: Analysis of Sample Fire Whirl Frame, Outline shown in orange and blue show the right and left edges of the flame for the intents of image analysis calculations. Walls shown are 55 cm high

Chapter 4: Results

Experimental results are presented here where the wall height of a fire whirl generator was varied from 0 to 55 cm above the fuel surface. Measurements such as changes in mass loss rate, flame height and length, and inflow velocities for different wall heights are presented.

4.1 Visual Observations

Once the heptane in the fuel pan is ignited by a propane torch, the resulting flame would quickly spread over the pool and elongate as the whole pool surface began to burn, shown in Figure 4.1A. As the flame developed it would stretch in one direction and the "tongue" of the flame at the tip would sweep clockwise around the enclosure, similar to the inclined flame shape mentioned in [28]. This inclined flame shape is shown in Figure 4.1B. For the lower wall heights or particularly unstable tests, this would be the full extent of flame behavior. For greater wall heights, the tip of the flame tongue would begin to curl in on itself and form a structure similar to a small fire whirl, precessing far off source of the fuel. This small structure resembled a small fire whirl with the flame sheet not quite wrapping around a full cylinder. This behavior can be seen in Figure 4.1C, though the structure is difficult to discern in a still image. The small fire whirl structure at the tip of the flame would precess as the flame tongue swept across the enclosure floor. This structure would occasionally precess over the fuel source, lengthening into a full fire whirl, but this would

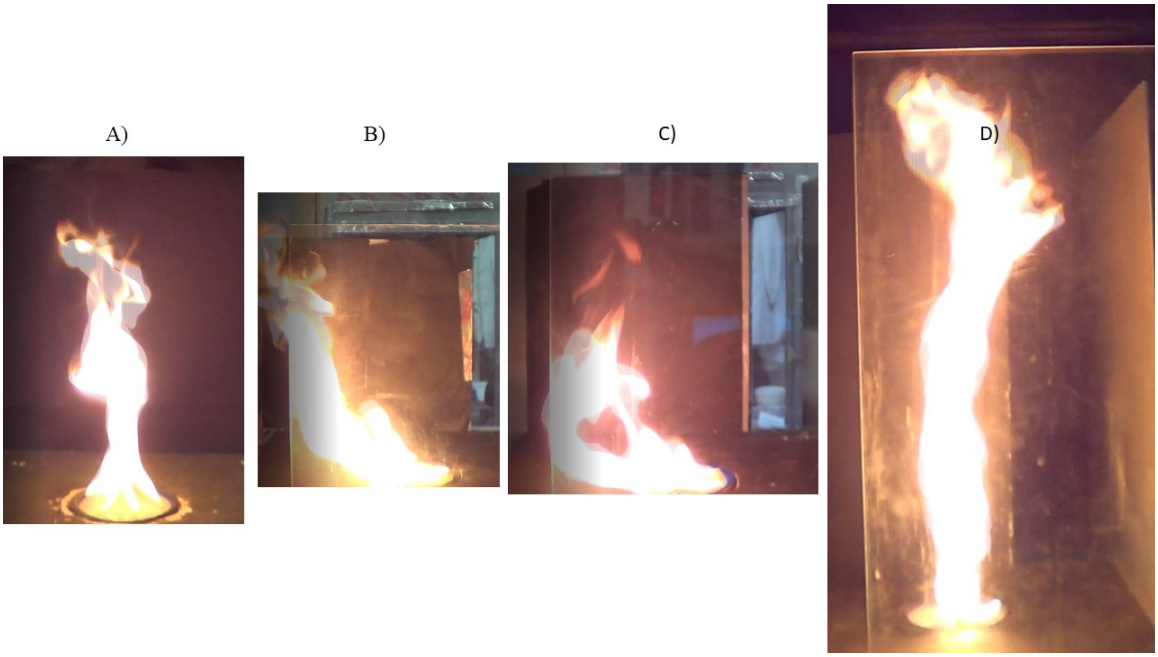

Figure 4.1: Representative images taken from side-view video frames of A) a pool fire formed at initial ignition or low wall heights B) an inclined flame formed during partial swirling but no fire whirl formation C) an inclined flame showing curling at the flame tip and D) a fire whirl. Images are scaled such that the fuel dish diameter is approximately equal in all frames.

not always result in a stable formation. For the largest wall heights (45 or 55 cm), the flame would become a rotating inclined flame early in the progression of the experiments, and the rotation would accelerate until the flame curled at the tip and quickly stabilized over the fuel source. The stable fire whirl is shown to scale in Figure 4.1D compared with the pool fire and inclined flame.

4.2 Mass Loss Rate

The mass loss rate for each test was calculated by tracking the instantaneous mass recorded by the load cell placed under the fuel dish during each test and then calculating the difference in mass at each time step. The results of these tests also unavoidably include some amount of mass lost due to the evaporation of the water layer below the fuel, though

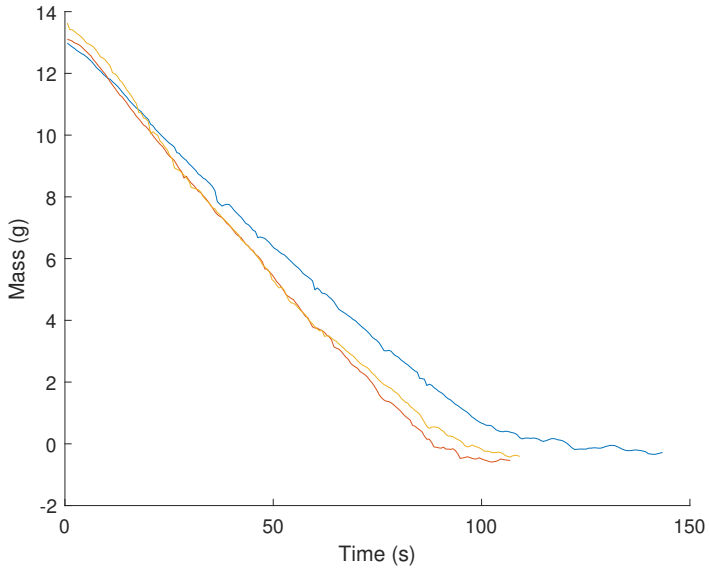

Figure 4.2: Instantaneous mass recorded by the load cell with an effective wall height of 20 cm and a gap size of 10.5 cm

in all tests this value was less than 1 gram, and was less than 0.5 grams for the majority of tests. An example of the mass recorded by the load cell is shown in Figure 4.2 for a test condition with a 20 cm wall height and 10.5 cm gap size. For comparison, the instantaneous mass recorded by the load cell for multiple tests with a wall height of 55 cm is shown in Figure 4.3. In Figure 4.3, one test is shown with a much more gradual slope that transitions to a higher slope as time progresses; this is indicative of a test where the fire whirl did not form until late in the test, causing the delayed increase in mass loss rate. As can be seen in these figures, the mass loss rate appears to be steady with the exception of noise in the signal and instances of delayed fire whirl formation.

The mass loss rate for each test was taken as a finite difference between the mass at each time step at a frequency of approximately 1.75 Hz. Figure 4.4 shows the mass loss calculated this way for the duration of a representative test with a wall height of 15 cm. As can be seen from this figure, the mass loss rate quickly reaches a steady state with tails before ignition and after extinction. These tails were removed in order to create an average

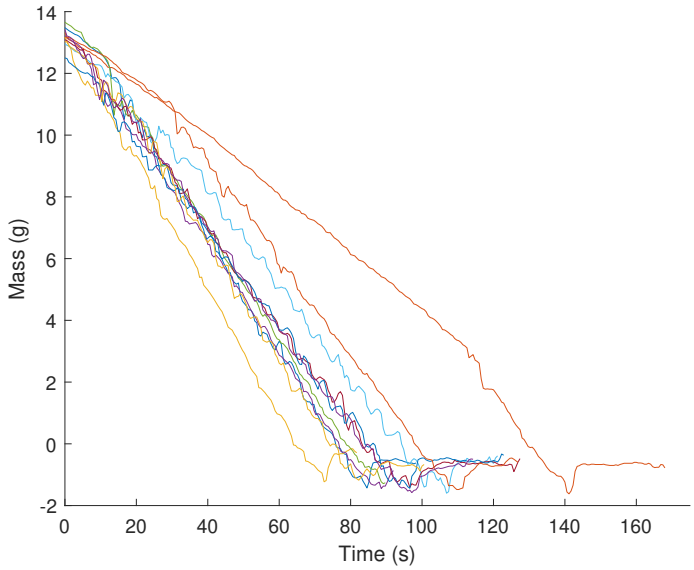

Figure 4.3: Instantaneous mass recorded by the load cell for repeated tests with an effective wall height of 55 cm and a gap size of 10.5 cm

mass loss rate for each test, equivalent to drawing a line of fit across the steady burning region. For the purpose of this calculation, the tails were taken to be any mass loss rate lower than 10% of the peak mass loss rate and as such these values were not included in the calculation of the overall average mass loss rate for each test.

The mass loss rate calculated in the previously-described way is shown for each test as a function of wall height in Figure 4.5. As can be seen in the figure, measurements of mass loss rate are relatively repeatable for many configurations; however, for some wall heights there is extreme variability, especially when the flame tilts and precesses, sometimes but not always transitioning into a fire whirl. Regardless of variability, there is a strong trend that mass-loss rate almost doubles with any level of wall height.

Figure 4.6 shows the average mass loss rate for each wall height with two standard errors denoted by error bars on each point. Two outliers from Figure 4.5 that lied beyond 240% of the mean (at the 40 cm wall height) were removed as they were caused by equipment malfunction. The mass loss rate increases with wall height for the first three points of

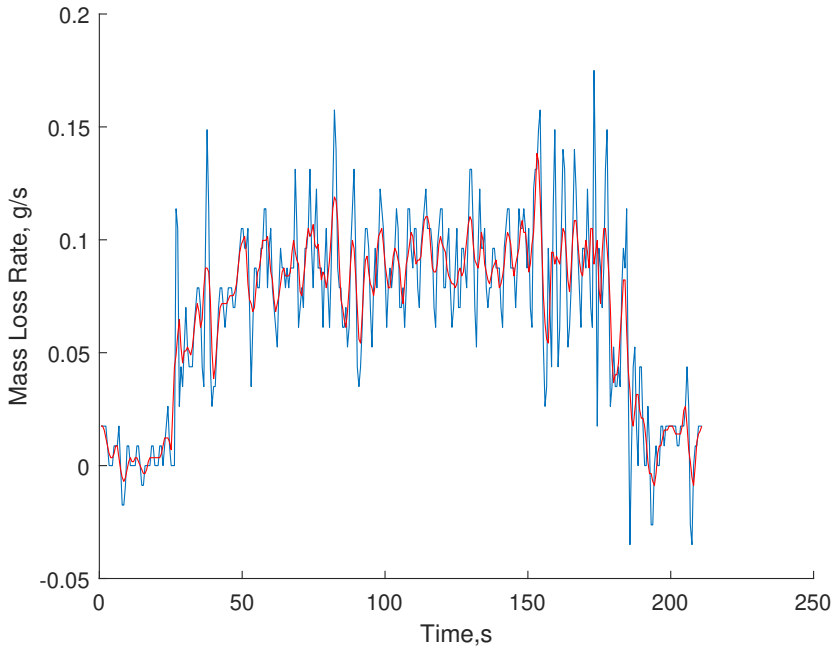

Figure 4.4: The mass loss rate calculated over a test duration with a wall height $W = 15$ cm. A five point moving average is applied to the raw finite-difference and is shown overlayed in red

Figure 4.6, then plateaus, showing a mass loss rate of double that of a pool fire with walls as low as 10 cm.

4.3 Flame Length

The flame length was calculated for each video frame from ignition to extinction by taking the diagonal distance from the flame tip to the center of the fuel dish. An example of the instantaneous flame lengths measured is shown in Figure 4.7. It shows an initial region without stable fire whirl formation followed by clear fire whirl formation with a relatively steady flame height throughout the remainder of the test duration. This flame length was chosen to be represented instead of the strictly vertical flame "height" due to difficulties capturing the height of the flame when tilted due to unsteady formation of the

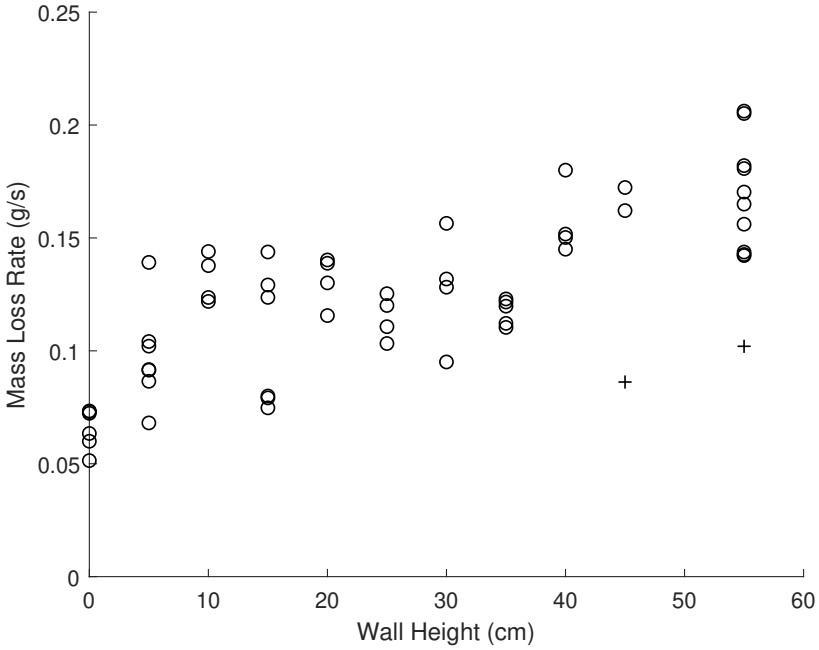

Figure 4.5: Mass loss rate as a function of wall height for each test. Unsteady pool fires at large wall heights that never formed stable fire whirls are marked as crosses rather than circles.

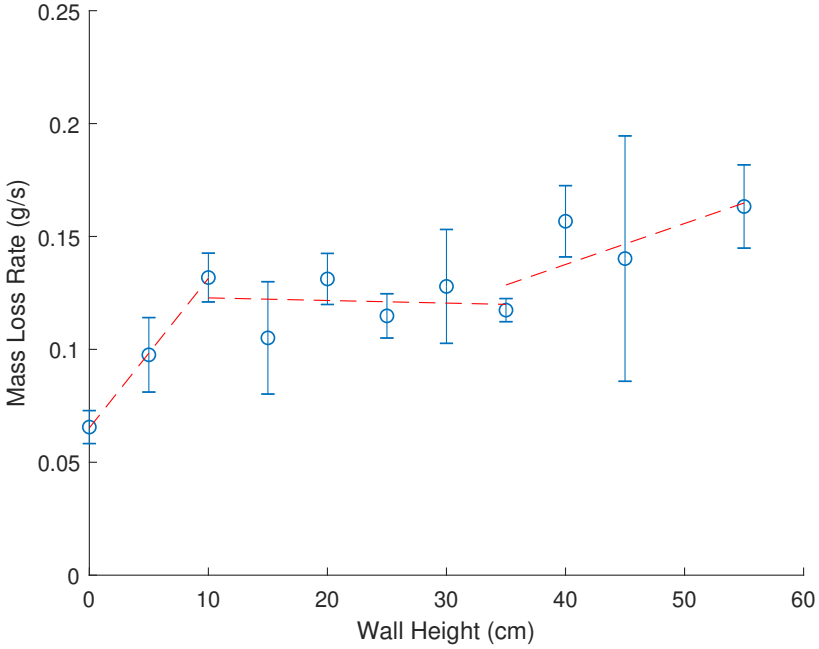

Figure 4.6: Mass loss rate as a function of wall height shown with two standard errors.

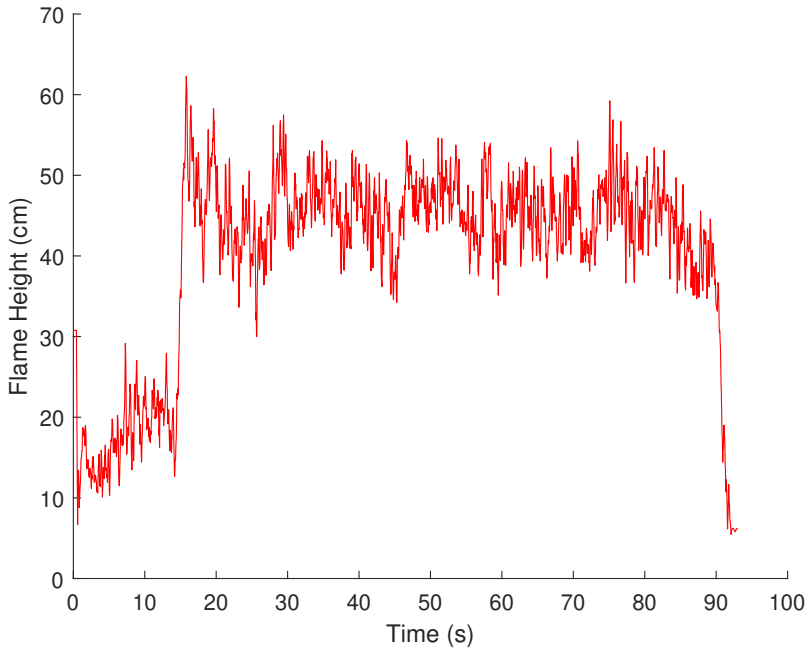

Figure 4.7: Instantaneous flame height for a test duration with conditions $W = 55$ cm smoothed by 5-point moving average

fire whirl. The fire whirl stabilizes over time, progressing through an inclined flame stage not dissimilar to the inclined flames in [28].

The variation in flame length for each test condition is shown in Figures 4.8 and 4.9, with the former showing time-averaged flame heights for individual tests and the latter averages of these values and associated variations between tests. As can be seen, there is a significant increase in flame height with increasing wall height. This is most significant as the wall height increases over 35 cm, indicating some transition that results in significant increases in flame length. Increased variation in flame length occurs at higher wall heights due to variations in the time that it takes for fire whirl formation to occur, or whether fire whirl formation occurs at all. At wall heights of 45 and 55 cm, for instance, one test is recorded where fire whirl formation does not occur, offering dramatically lower flame lengths. These two tests are excluded as outliers from Figure 4.9.

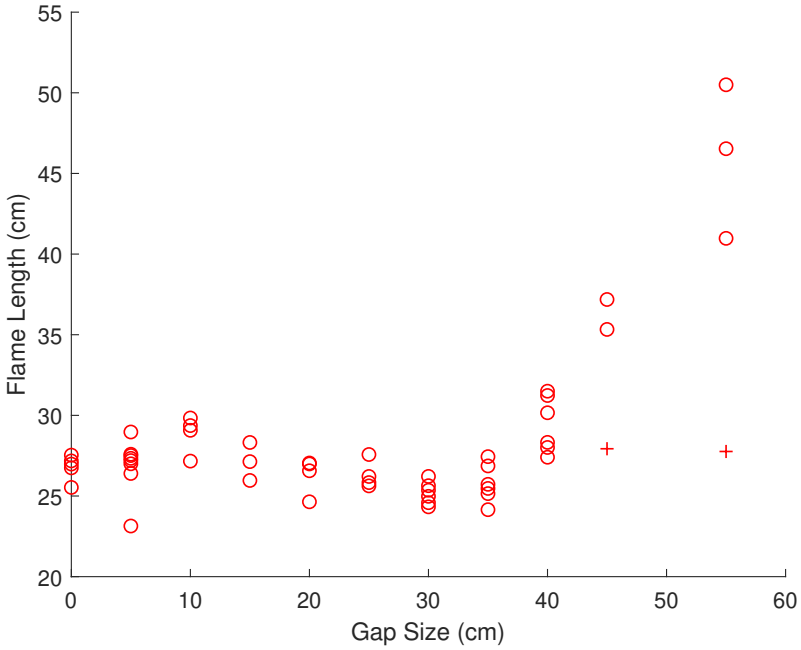

Figure 4.8: Variation of flame length with wall height with a fixed $G = 10.5$ cm. Unsteady pool fires at large wall heights that never formed stable fire whirls are marked as crosses rather than circles.

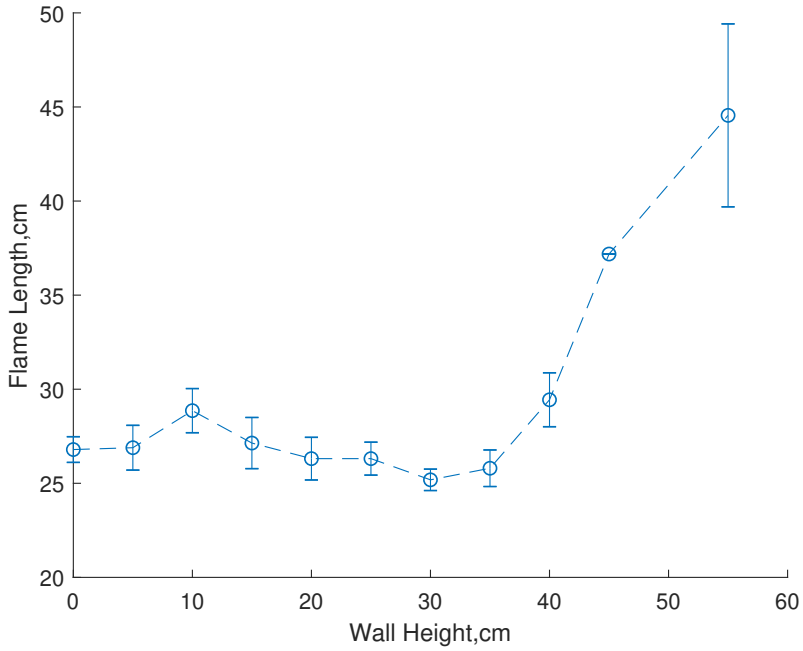

Figure 4.9: Variation of flame length with wall height with a fixed $G = 10.5$ cm. Error boars shown represent two standard deviations. Tests with wall heights higher than 35 cm that did not form fire whirls were considered outliers and not included in this plot

For perspective, a comparison of the flame length to the flame height is shown in Figure 4.10, which depicts the average ratio of flame length to flame height. As can be seen, the flame length is often slightly longer than the flame height due to tilting of the flame, which increases with intermediate wall heights where the flame experiences more tilting and precession. The large variation observed at a 55 cm wall height is due to the presence of the flame that never developed beyond the inclined flame stage as mentioned previously.

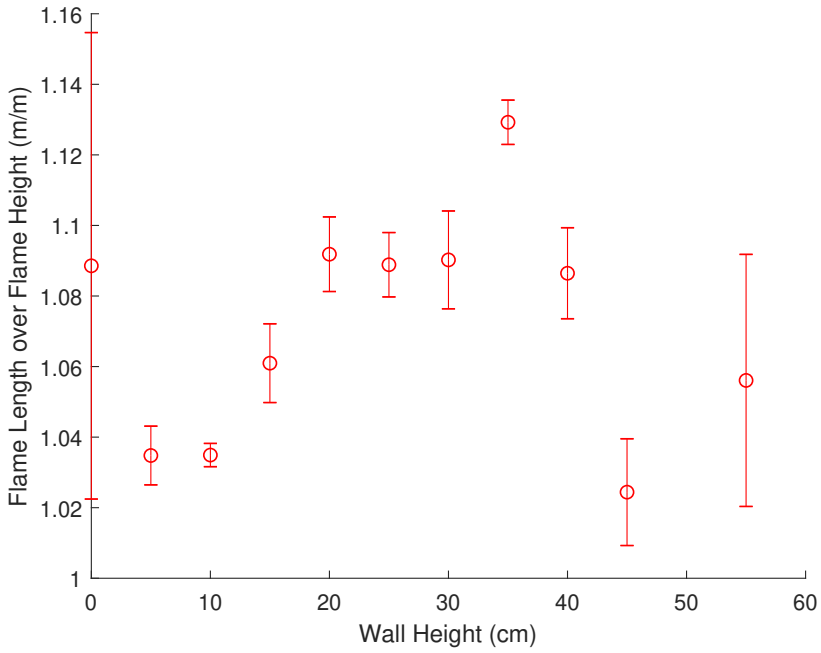

Figure 4.10: Flame length vs. flame height ratio for all wall heights with a fixed gap size $G = 10.5$ cm

The width of the flame was also calculated in a similar means as flame height and length, although the width was measured at each pixel height and averaged along the entire length of the flame. The resulting flame widths are shown in Figure 4.11. As the flame extends and forms a more concentrated vortex with increasing wall heights the width of the flame decreases. Fire whirls, interestingly, are shown to have greater flame widths than pool fires, perhaps because pool fires have a width that is about the pool diameter at

the base, decreasing with height, while the fire whirl forms a cylindrical vortex of nearly-uniform width. Effects that spread out the flame, such as tilting and precessing as the flame transitions but is not fully a fire whirl may be responsible for much of this increase at lower wall heights.

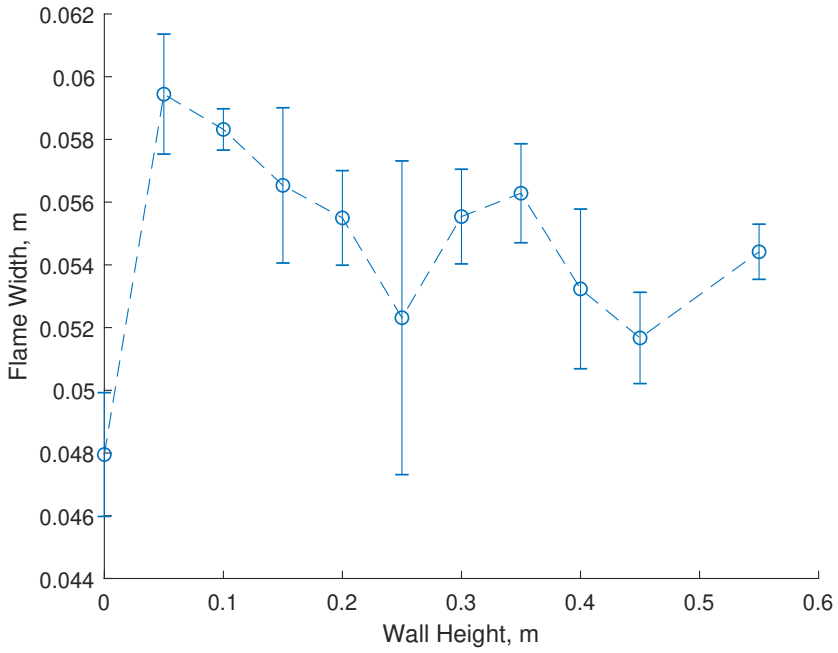

Figure 4.11: Flame Width as a function of Wall Height

The tilt of the flame was also calculated from the difference between the diagonal line from the center of the fuel pool to the flame tip and the line perpendicular to the base plate, shown as a function of wall height in Figure 4.12. Initially the flame remains fairly vertical, although with larger wall heights increased tangential momentum elongates and tilts the flame as it precesses around the chamber. At a critical wall height, about 35 cm in this study, a peak tilt angle is found, after which the fire whirl tilt dramatically decreases and a relatively stationary, vertical fire whirl is stably formed.

As mentioned earlier, fire whirls often precess around the base of a formation apparatus, especially in transition regimes. This was observed in this study as well. The bottom

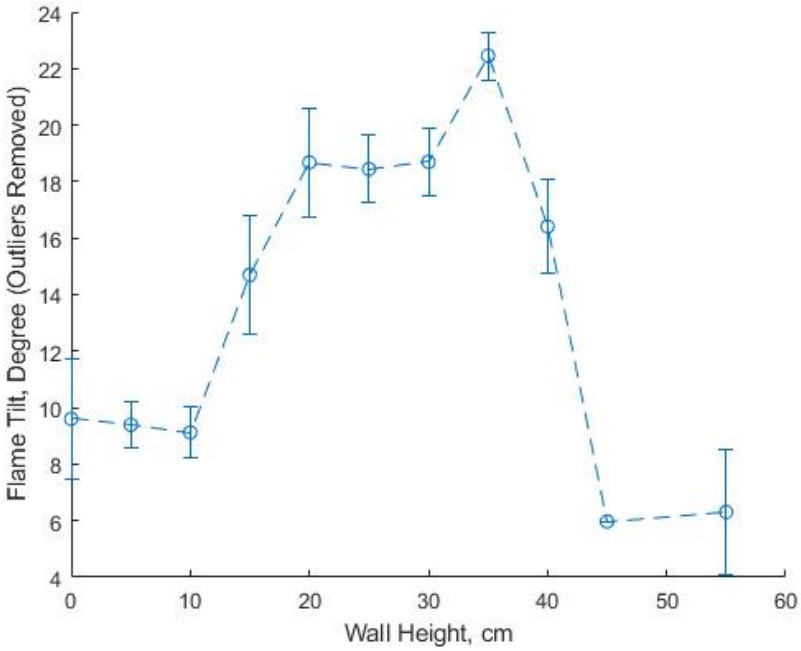

Figure 4.12: Angle of tilt of the flame length, same outliers removed as in Figure 4.9

centimeter of flame was considered the base of the flame, and its horizontal location compared to the center of the fuel pool was considered the radius of precession of the flame. The resulting radius of flame precession from each test is shown in Figure 4.13. No trends were clearly found with this value, suggesting all fire whirls generally precessed around the base of the apparatus in a somewhat similar fashion.

The gap size was also varied from 10.5 cm with a fixed wall height of 55 cm to see the effects of gap size on the flame height and mass loss rate. The variation in flame length is shown in Figure 4.14. The smallest gap size tested was 5 cm and did not form a stable fire whirl. While the gap size may have a slight effect on resulting flame length, for the gaps studied there was little difference between 10.5 and 12.5 cm. Figure 4.15 shows the variation in burning rate for these gap sizes, with the 10.5 and 12.5 cm gap sizes having very similar burning rates and the 5 cm gap size with a lower burning rate, likely due to the lack of fire whirl formation in those tests. Further results from the variation of gap sizes

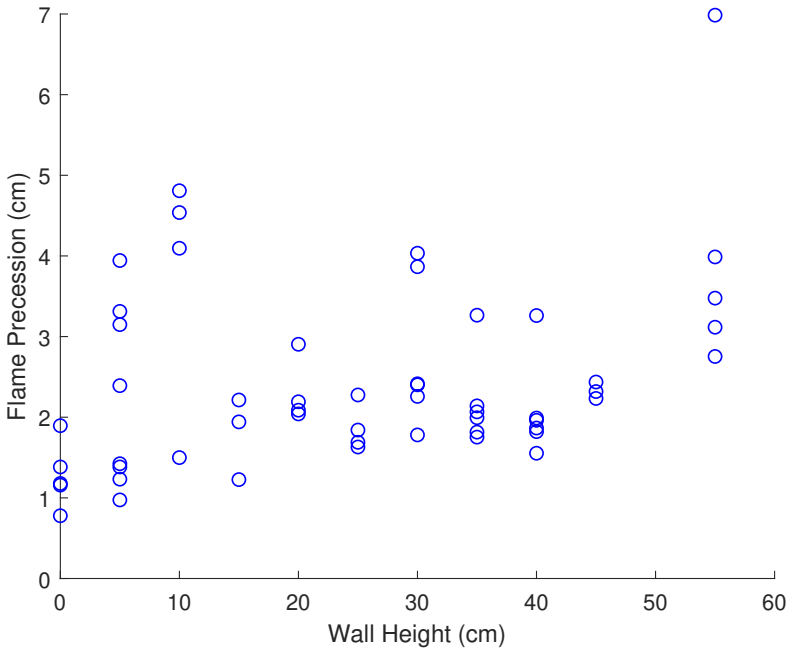

Figure 4.13: Radius of flame precession as a function of wall height

are shown in the appendix.

4.4 Velocity

Fire whirl formation is often characterized by a balance between tangential circulation and buoyant momentum driven by the heat release rate. Measurement of tangential velocity can help estimate this circulation. The velocity of the entrained air at the inlet was measured for the case of 55 cm high walls with a 10.5 cm wide gap at several heights along the gap. Figure 4.16 shows the velocity at varied heights along the wall along the center of the gap. The velocity is also shown along the centerline of the inlet gap for a wall height of 15 cm in Figure 4.17. For both configurations inlet velocities occur on the order of 0.15 - 0.2 m/s, slightly lower than the 0.4 - 0.6 m/s average found for a fire whirl by Hu et al. [29], although the gap size and scale are different. As expected, the velocity is slightly lower at

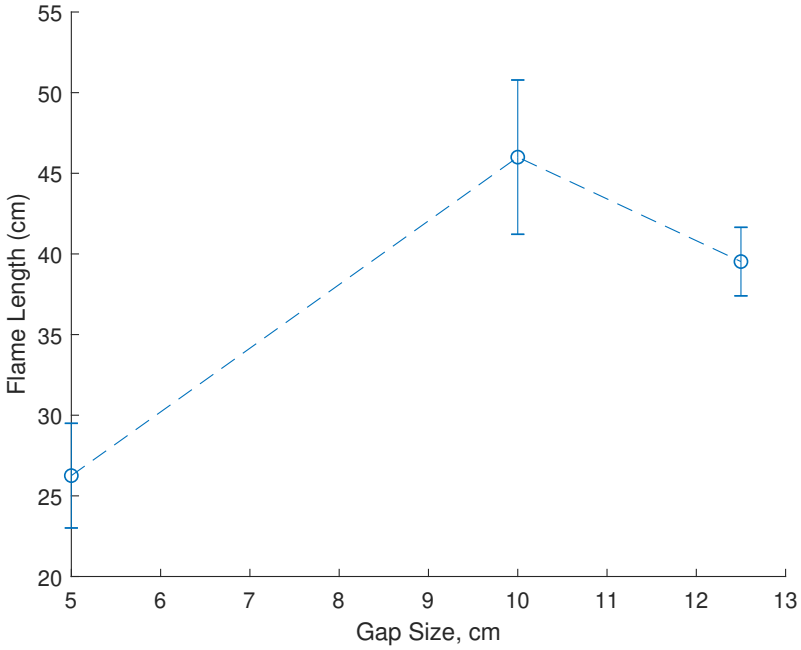

Figure 4.14: Variation of flame length with changes in inflow gap size for a fixed wall height of 55 cm.

the base of the apparatus where a boundary layer is likely present.

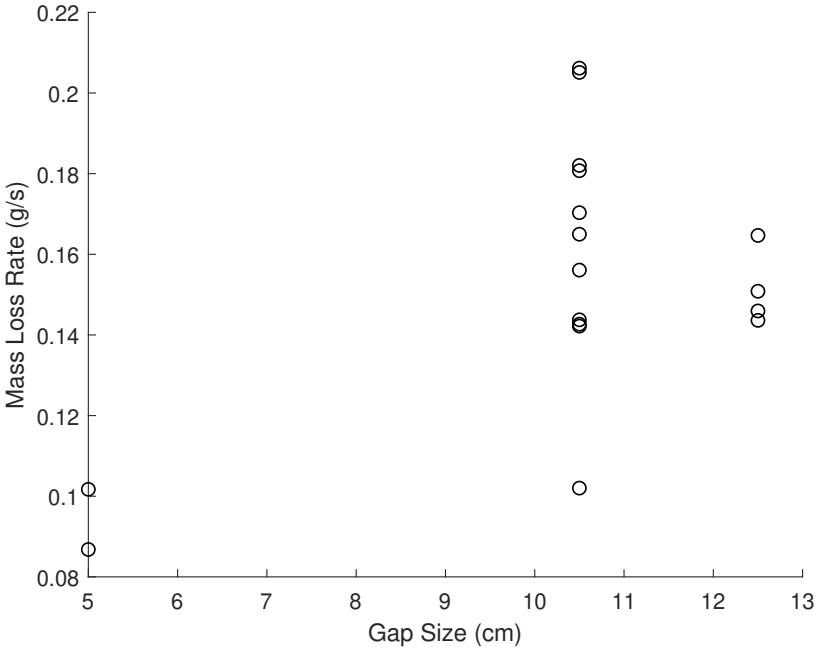

Figure 4.15: Variation of burning rate with changes in inflow gap size for a fixed wall height of 55 cm.

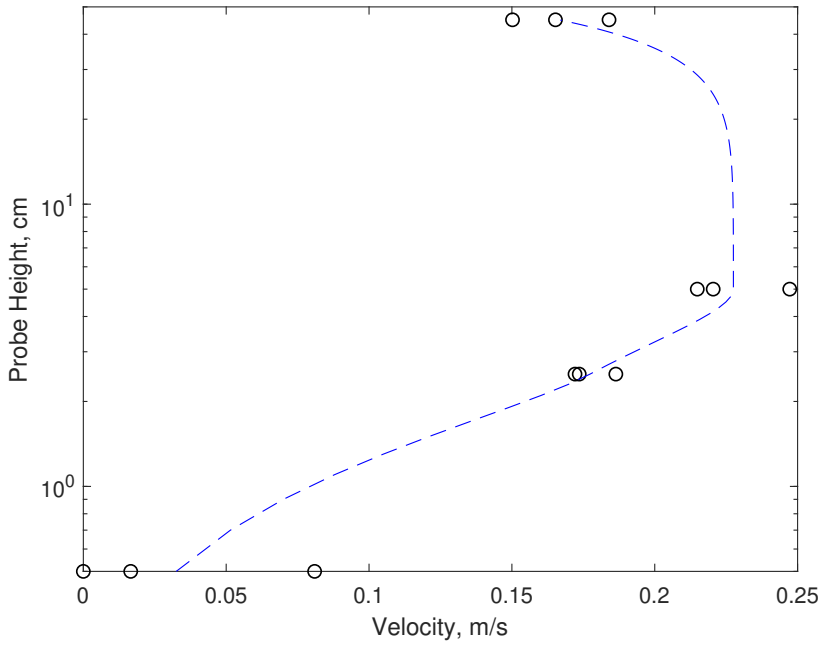

Figure 4.16: Velocity along the height of an inlet gap shown on a logarithmic profile, $G = 10.5$ cm, $W = 55$ cm, probe heights at 0.5, 2.5, 5, and 45 cm, with a smoothed dashed line shown fit to the average profile.

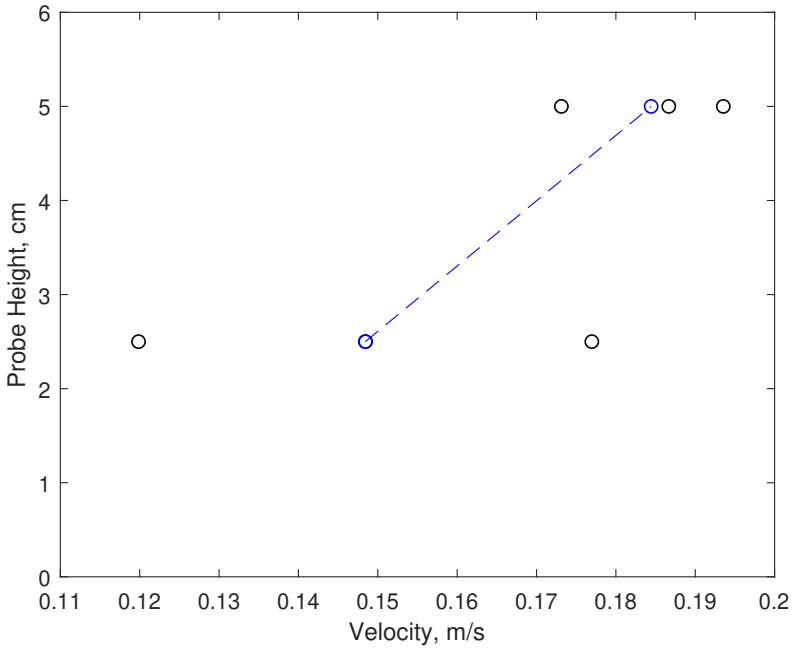

Figure 4.17: Velocity along the height of an inlet gap shown on a logarithmic profile, $G = 10.5$ cm $W = 15$ cm

Chapter 5: Discussion and Analysis

5.1 Discussion

As shown in Figure 4.6, the addition of even short walls cause an increase in the burning rate of the fuel, with walls as short as 10 cm, less than one diameter of the fuel dish, causing an increase in burning rate of close to double. This may show that the increase in burning rate depends only on the formation of an inflow boundary layer over the fuel surface, pushing the flame closer to the fuel surface increasing convective heat transfer, and that the shorter walls suffice to induce this small amount of circulation.

Figure 4.9 shows that flame height tends to increase as the wall height increases. However, the mass loss rate does not increase at the same rate as the wall height increases, as shown in Figure 4.6, suggesting that the increase in flame height is due to fluid dynamics effects rather than an increase in the burning rate of the fuel. This is further supported by Figure 5.1, which shows two distinct regions, one where the heat release rate increases without effecting the flame height, and one where the flame height increases without increase in the heat release rate. The two distinct regions ($FL < 0.3$ m and $FL > 0.3$ m in height) indicate that there is a critical point separating the fire whirl and pool fire regimes, rather than a smooth transition as wall height increases. This critical value of transition is shown in Figure 5.1 by the outlined regions, with the red dotted outline showing the pool fire and inclined flame region and the blue dashed outline showing the fire whirl region. The heat release rate was calculated for Figure 5.1 as the average mass loss rate for each

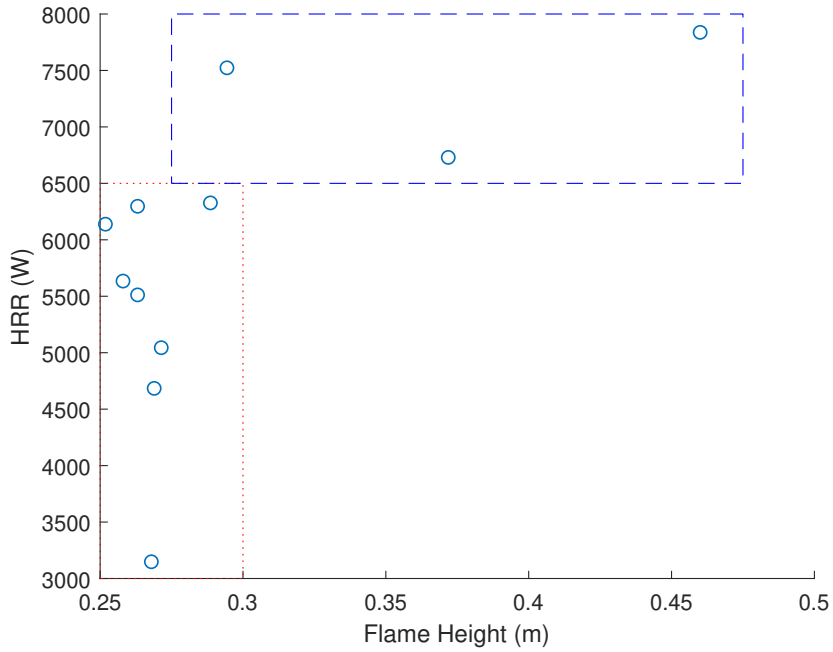

Figure 5.1: Heat Release Rate as a function of Flame Height. The red dotted outline show the pool fire and inclined flame; fire whirls are shown in the region outlined in blue dashes

condition times a constant heat of combustion, taken to be 48×10^3 kJ/kg. The existence of a critical dependence on wall height is interesting considering that fire whirls are dominated by the boundary layer conditions at the base [13]. The walls of the structure could either be creating a pressure difference akin to the stack effect to increase the boundary layer flow or, perhaps the pressure difference inside the generator, due to the buoyant plume, is entraining air from along a greater portion of the flame length, and the walls are restraining the flow to shear the buoyant column. Further experiments and simulations directly observing this airflow will be necessary to further understand this effect.

The tilt of the flame reaches a maximum at a wall height of 35 cm, as shown in Figure 4.12. This correlates with the formation of fire whirls beyond this height, as shown by the increase in flame height in Figure 4.8. Figure 4.12 illustrates the regions discussed in Section 4.1. The small stable region with wall height at or below 10 cm corresponds to a

pool fire with very low circulation. The region with increasing degree of tilt represents the inclined fire such as that discussed by Lei et al. [28], [33]. The second stable region appears to correlate with the region where the flame stabilizes perpendicular to the fuel surface.

The precession observed over the fuel pool appears independent of the effective wall height, as shown in Figure 4.13. The slight decrease in fire whirl width with a corresponding increase in the heat release rate of the fire whirl seems to agree with the simple scaling analysis of a momentum-controlled fire whirl presented by Chuah, Kuwana, and Saito [19]. Though Satoh and Yang's simulations of self-entrained fire whirls [31] assume a much larger enclosure, the velocity measurements taken in this experiment appear similar to the simulated value and qualitatively have a similar profile.

5.2 Analysis

Heat release rate is often represented in the analysis of fire plumes with a nondimensional value, Q^*, calculated here as

$$Q^* = \frac{\dot{m}\Delta H}{C_p \rho \Delta T L_h^2 \sqrt{gH}}, \tag{5.1}$$

where C_p is the specific heat of ambient air, ρ is the density of ambient air, ΔT is the difference in temperature between the adiabatic flame temperature of heptane and the ambient temperature, ΔH_c is the heat of combustion of heptane, $\dot{m}$ is the mass loss rate, L_h is the horizontal length scale, and H is the vertical length scale. This scheme of nondimensionalizing heat release rate uses two separate length scales, one horizontal length scale to represent the size of the flame or fuel pool, while the vertical length scale is used in the radical to create a representative axial velocity. Figure 5.2 shows Q^* as a function of the wall height, with $L_h = w_f$ the flame width, and $H = L$ the flame length. Figure 5.3 also shows Q^* as a

function of wall height, but with the horizontal length scale $L_h = D_0$ the fuel dish diameter.

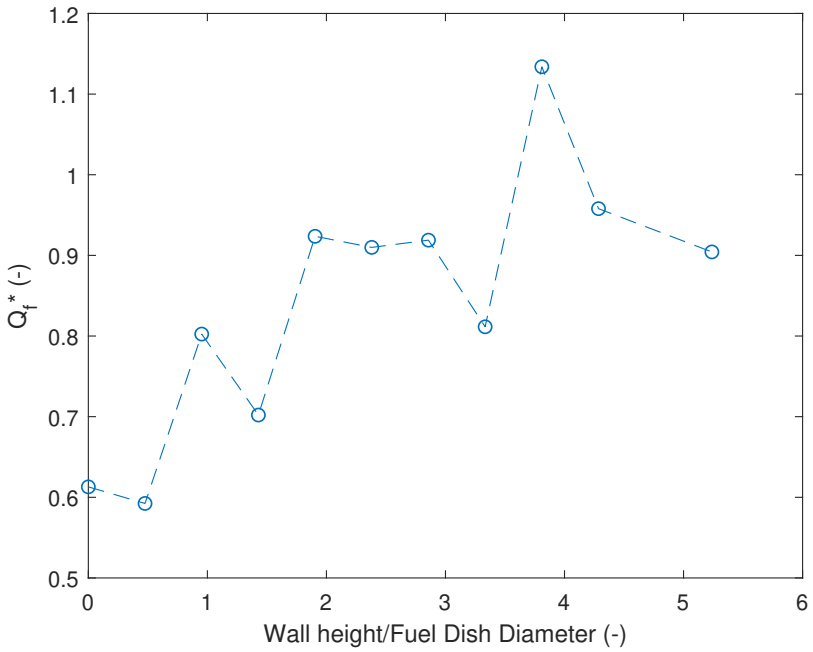

Figure 5.2: Heat Release Rate nondimensionalized by flame characteristics, Q_f^* vs Wall Height in terms of fuel dish diameter

The value of L^*, the nondimensional flame length, was calculated as

$$L^* = L/L_s, \tag{5.2}$$

where L is the flame length and L_s is a scaling length, either the width of the flame, w_f or the width of the fuel dish D_0. Figure 5.4 shows L^* as a function of wall height with $L_s = w_f$ on a logarithmic y-axis. Figure 5.5 shows the flame length as a function of the wall height, both in terms of the fuel dish diameter. The flame length over fuel dish diameter shown in Figure 5.5 shows that the flame height remains relatively steady for wall heights of 35 cm or lower, and only shows an increasing trend when the fire whirl is formed. The ratio of flame length to flame width, L_f, as shown in Figure 5.4 shows the variations in flame geometry introduced by the changing wall height.

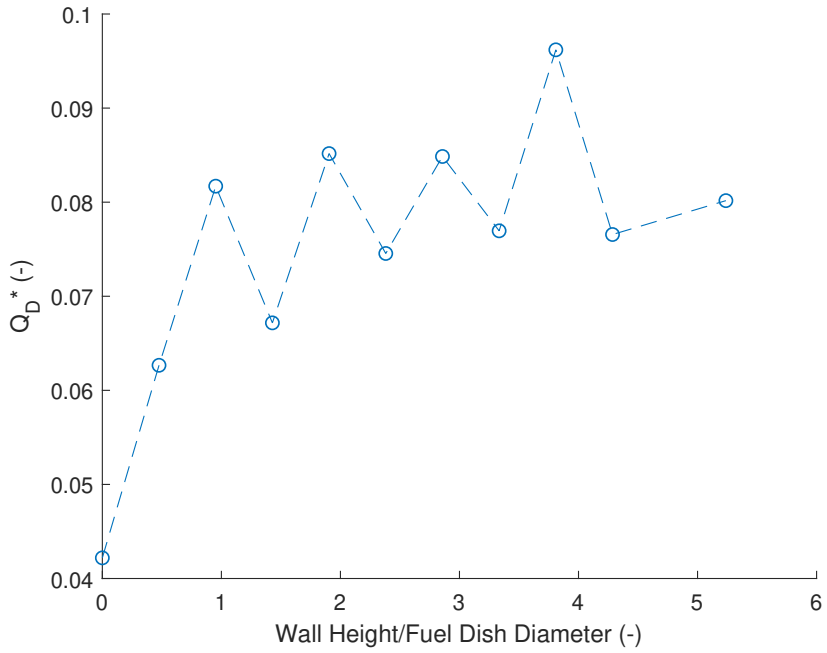

Figure 5.3: Heat release rate nondimensionalized by fuel dish diameter, Q_d^* vs wall height in terms of fuel dish diameter.

Figure 5.6 shows the dimensionless flame length as a function of the dimensionless heat release rate. The points at wall heights up to and including 40 cm are shown with red crosses, while points at wall heights from 40 cm to 55 cm are shown with blue circles, each with a color-coded first-order line of best fit. The point at a wall height of 40 cm was included in both groups as it appears to be the transition point between the pool fire and fire whirl regimes. This makes clear that the regime shift occurs at a critical point rather than any gradual transition. As Dobashi et al. [22] and Kuwana et al. [23] scale the flame length with the Péclet number, a representative Péclet number was calculated for each wall height using equation 5.3

$$Pe = \frac{\dot{m}}{\rho_a w_f D_s} \tag{5.3}$$

where $\dot{m}$ is the mass loss rate, ρ_a is the density of ambient air, w_f is the flame width, and D_s is the coefficient of molecular diffusion for n-heptane in air. Figure 5.7 shows the Péclet

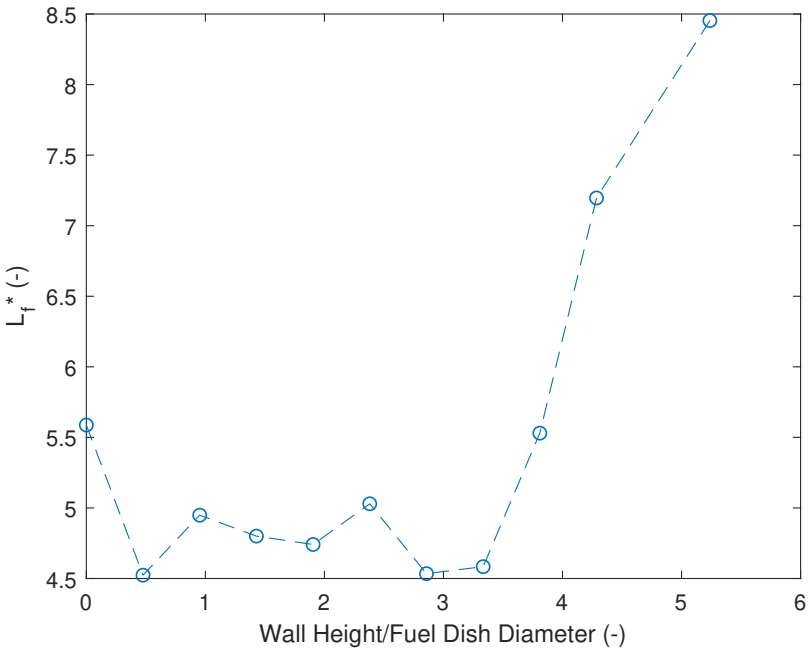

Figure 5.4: Flame Length nondimensionalized by flame width, L_f^*, as a function of wall height in units of fuel dish diameter, W/D

number calculated as a function of wall height, with a power law, $Pe = 0.00249(W/D_0)^{0.232}$ fit to the data with an $R^2 = 0.66$. This power law was the best fit for all data above the pool fire results at $W = 0cm$, and the lack of y-intercept in using this model was accepted as for this analysis the pool fire was considered a separate regime from the inclined and whirling flames. Figure 5.8 shows the flame length as a function of the Péclet number, with points below 40 cm as red crosses and above as blue circles. Compared to the Péclet number scales in Dobashi et al. [22] and Kuwana et al. [23], the points below the 40 cm threshold do not constitute a fire whirl, and the points above this threshold are too sparse to note whether the trend appears to follow the trend in the cited works. Dobashi et al. [22] note that their correlation between L/D_0 only hold for laminar flames with fuel sources of less than 5 cm diameter, which is exceeded in these experiments.

Figure 5.9 shows the ratio of the flame length to the burning rate as a function of the

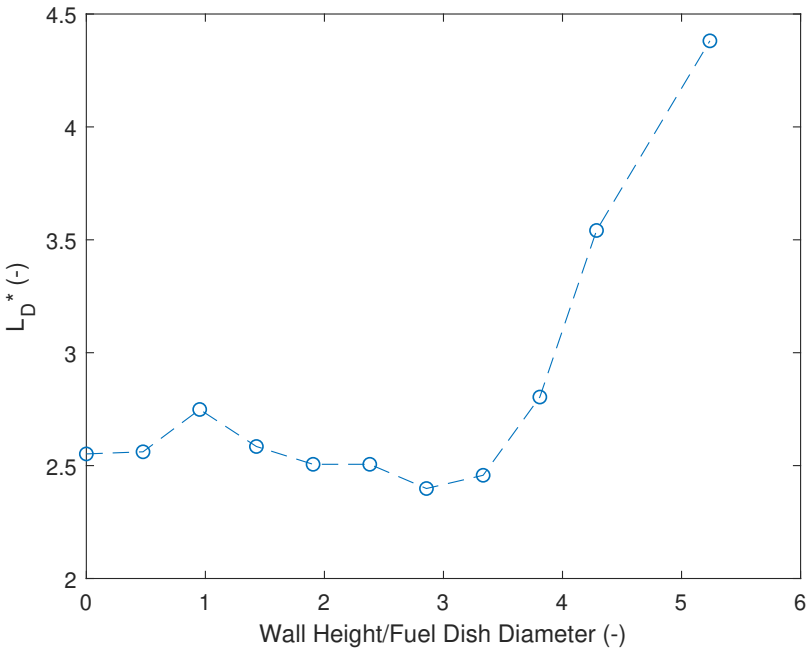

Figure 5.5: Flame Length in units of fuel dish diameters, L_D^*, as a function of wall height in units of fuel dish diameter, W/D

wall height in terms of fuel dish diameter. The value of L^*/Q^* was calculated as

$$L^*/Q^* = \frac{C_p \rho \Delta T g^{0.5} D_0}{\Delta H_c} \frac{L^{3/2}}{\dot{m}} \tag{5.4}$$

where C_p is the specific heat of ambient air, ρ is the density of ambient air, ΔT is the difference in temperature between the adiabatic flame temperature of heptane and the ambient temperature, ΔH_c is the heat of combustion of Heptane, L is the flame length, D_0 is the fuel dish diameter, and $\dot{m}$ is the mass loss rate. In equation 5.4, the fuel dish diameter is used as the characteristic horizontal length scale for the nondimensionalization of both L^* and Q^*. Figure 5.10, which shows a similar trend, uses the flame width as the characteristic horizontal length scale for both L^* and Q^*, calculated as

$$L^*/Q^* = \frac{C_p \rho \Delta T * g^{0.5} w_f}{\Delta H_c} \frac{L^{3/2}}{\dot{m}} \tag{5.5}$$

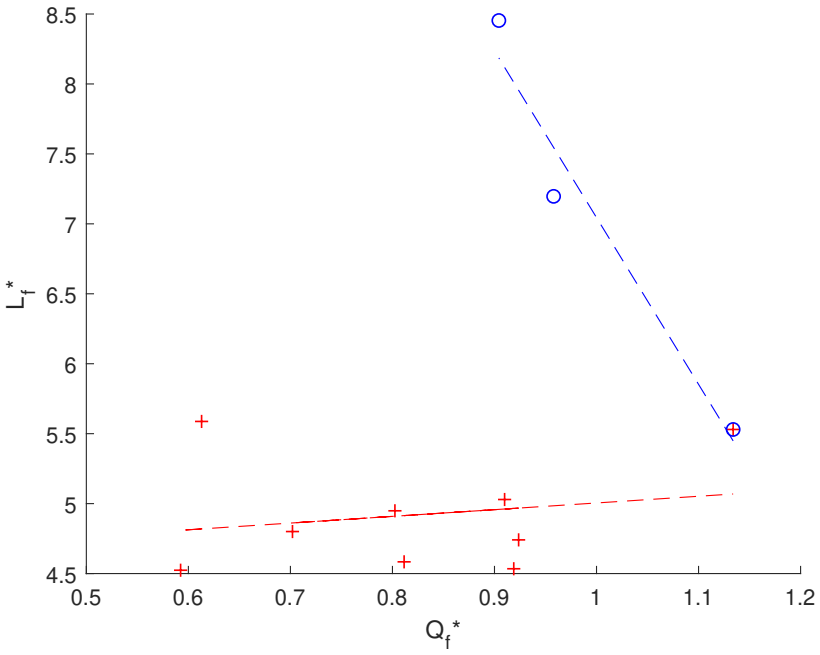

Figure 5.6: L^* by Q^*, $L_h = W_f$, data points corresponding to wall heights up to and including 40 cm shown in red crosses, data points corresponding to wall heights of 40, 45, and 55 cm shown in blue circles, both regions show with a line of best fit

where w_f is the width of the flame. For the interests of this investigation, a ratio of L^* and Q^* should be represented with the flame length characterized by the fuel dish diameter and the heat release rate characterized by the flame dimensions, described by Equation 5.6 and is shown in Figure 5.11,

$$L^*/Q^* = \frac{L}{D_0} \Big/ \frac{\dot{m} * \Delta H_c}{C_p * \rho * \Delta T * w_f^2 * g^{0.5} * L^{0.5}}. \tag{5.6}$$

Figures 5.9 to 5.11 show a decreasing trend in L^*/Q^* with the wall height, until the wall height surpasses a critical value similar to the value evident in Figure 4.12, as well as Figures 5.6-5.8, beyond which the trend increases sharply. This increase accounts for the increase in flame length due to the lengthening effects of the fire whirl. The increase in length-to-burning rate ratio indicates that the increase in flame length does not correspond

wholly to the burning rate enhancement and indicates aerodynamic control over the fire whirl's length once the wall height is beyond a critical value. This is supported by the simulations of Satoh and Yang [31], which seem to indicate that even in a self-entraining fire whirl, circulation becomes a dominant parameter for the fire whirl's characteristics.

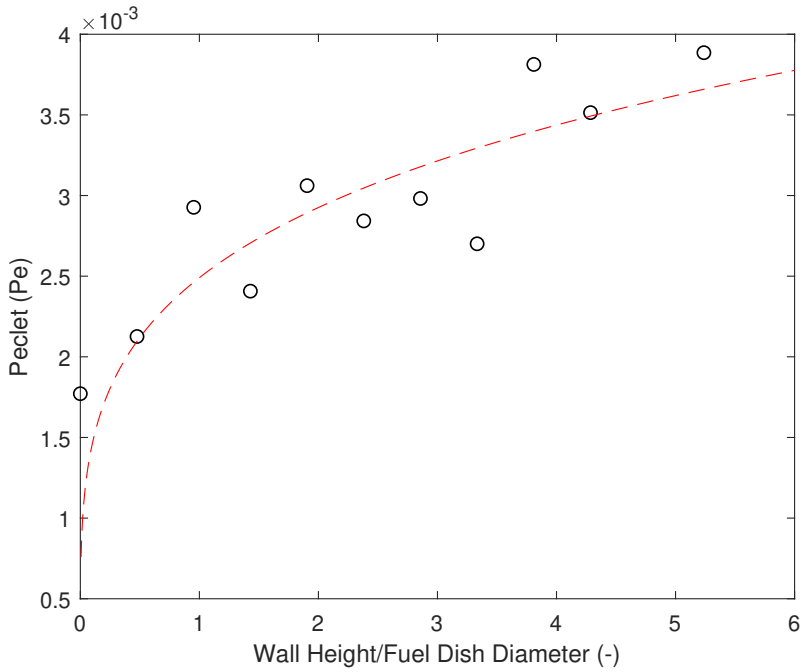

Figure 5.7: Péclet number as a function of wall height. Fuel dish diameter used as horizontal length scale, $Pe = 0.00249(\frac{W}{D_0})^{0.2323}$, $R^2 = 0.66$

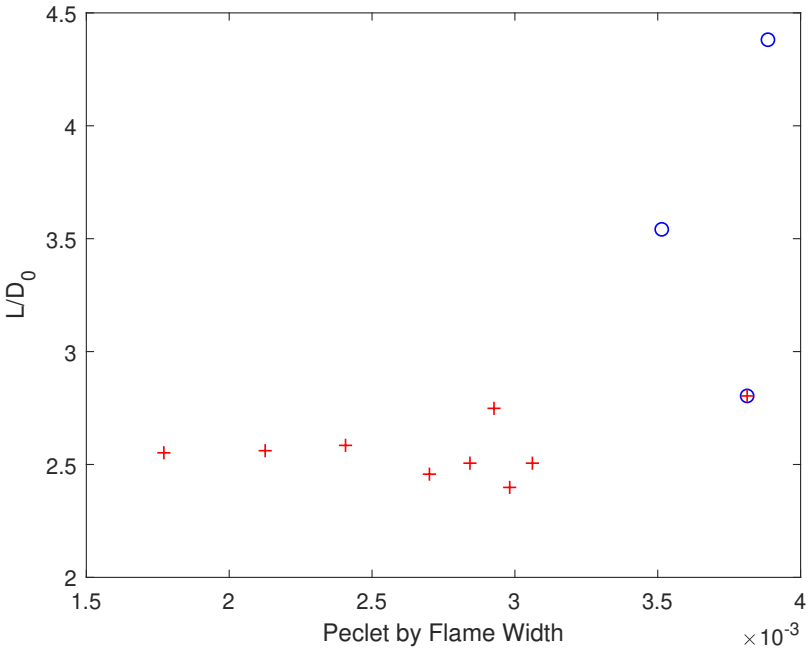

Figure 5.8: Flame Length over fuel dish diameter as a function of Péclet number. Red crosses represent data points corresponding to a wall height up to and including 40 cm, blue circles represent data points taken from wall heights 40, 45, and 55 cm

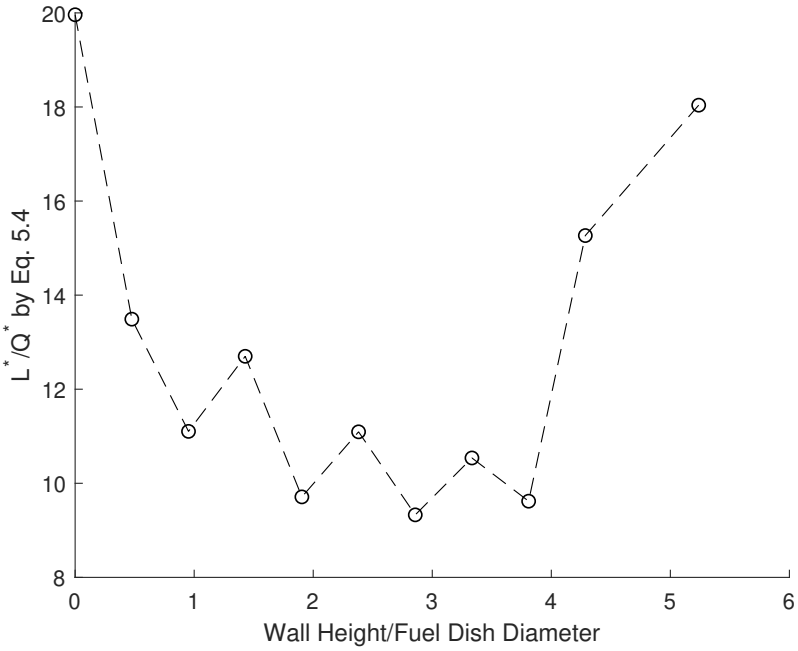

Figure 5.9: Dimensionless flame height to burning rate ratio as a function of wall height nondimensionalized by fuel dish diameter, with the fuel dish diameter as the characteristic horizontal length scale, as per Eq. 5.4

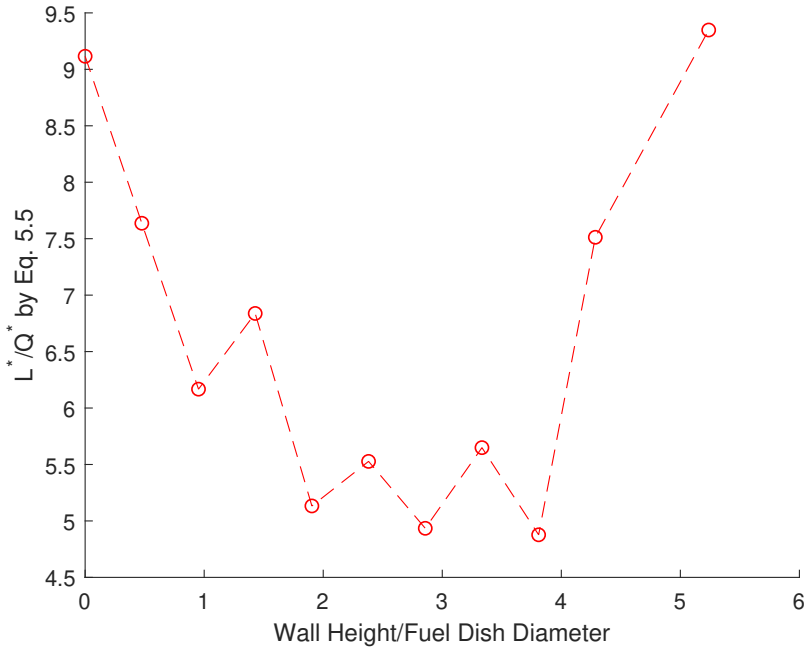

Figure 5.10: Dimensionless flame height to burning rate ratio as a function of wall height nondimensionalized by fuel dish diameter, with the flame width as the fharacteristic horizontal length scale, as per Eq. 5.5

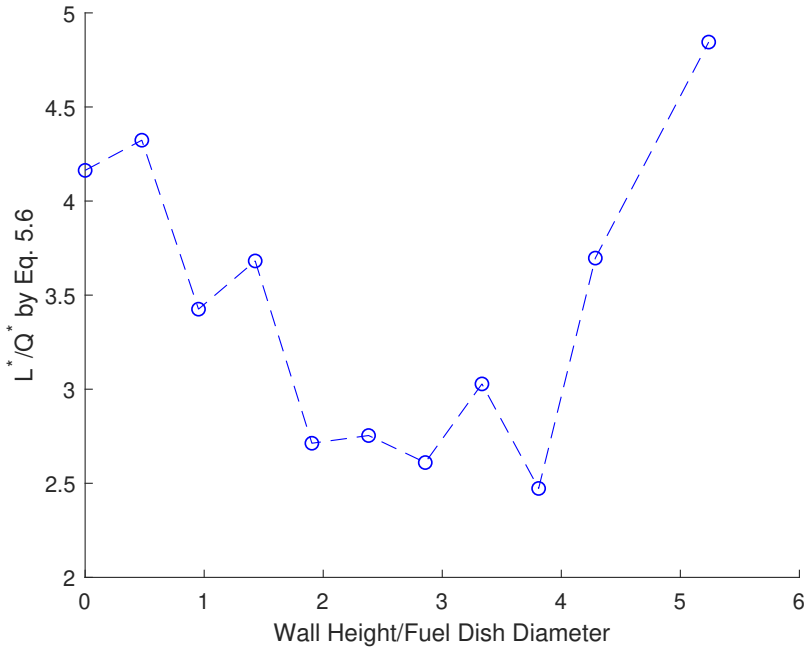

Figure 5.11: Dimensionless flame height to burning rate ratio as a function of wall height nondimensionalized by fuel dish diameter, with the flame length scaled by fuel dish diameter and heat release rate scaled by the flame dimensions, as per Eq. 5.6

Chapter 6: Conclusions and Future Work

Due to the circumstances caused by unprecedented global phenomena, many experiments intended to improve the resolution and extend the range of the data collected in this investigation had to be indefinitely postponed. This is not to say that the results and analysis of these experiments do not provide insight into the usage of fixed-frame fire whirl generators.

6.1 Conclusions

A range of effective wall heights were implemented in a fixed-frame fire whirl generator to investigate whether a stable fire whirl would be formed and the effects on the burning rate and flame length of the resulting fire whirl. Visually, the flame shape changed greatly with the increase in wall height. Walls with a height less than the fuel dish diameter produced little effect on the shape, with a strong resemblance to a pool fire, but with less noticeable periodic puffing action. With the introduction of even short walls, approximately $D_0 \leq W < 3.5D_0$, the flame began to incline and rotate across the interior of the generator. At the higher end of this range, the inclined flame showed a curling behavior at the tip. With walls beyond this height, $3.5D_0 \leq W$, the flame developed through the stages described previously to form a stable fire whirl. With the addition of walls with a wall height of only 10 cm, $W \approx D_0$, a near doubling of mass loss rate was seen. Further increases in wall height showed no increase in mass loss rate until the formation of the stable fire whirl, which then

showed a further slight increase in mass loss rate. This indicates that the bottom boundary layer is the primary effect increasing the mass loss rate in this configuration. This begs the question of the effects of this burning regime on emissions compared to a classical pool fire, as the flame length does not extend as one would expect with higher mass flux of fuel from the pool surface. The sudden increase in flame length with the formation of a stable fire whirl at a sufficient wall height, as well as the results of comparisons of nondimensional flame length and nondimensional heat release rate, shows a sharp regime change defined by a critical threshold wall height. For this investigation, the threshold wall height seemed to be between 35 and 40 cm or approximately 3.3 to 3.8 fuel dish diameters. As the flame length to burning rate ratio seems to increase with wall height once beyond this threshold, the fire whirl may be approaching a circulation-controlled regime of fire whirl.

6.2 Future Work

Due to unforeseen events putting an end to experimentation, some supplementary data useful to this investigation was not able to be collected. It is necessary to continue to investigate wall heights greater than 5 times the fuel dish diameter to confirm the trends shown in Figures 5.9 through 5.11. Additionally, higher resolution is needed to gather insight into the effects of the gap width on the formation of fire whirls in fixed frame generators. Importantly, velocity data would be needed to confirm the hypothesis presented regarding the inflow boundary layer and to provide a value for circulation that can be used in scaling analysis. If indeed the stack effect or turbulence suppression are the dominating factor in the formation and elongation of self-entraining fire whirls, the induced circulation must be quantified for analysis. For these experiments, the gap width approximately equalled the diameter of the fuel dish, so it is unclear whether the threshold wall height is dependent upon the diameter of the fuel dish or the gap width or a third parameter as yet unidentified.

The increase in mass loss rate with walls $W \approx D_0$ without equivalent increase in flame length raises questions as to the dependence of the mass loss rate on the inflow boundary layer as well as the emissions from this configuration. If, as is posited by Zhou et. al. [34], the inflow boundary provides enough access to air for complete combustion, then the emissions may not vary significantly in composition or quantity from each other, though they may meaningfully differ from a pool fire of similar size [6], but Lei et. al. [12] dispute the notion that the boundary layer inflow provides enough airflow for complete combustion at a large range of pool diameters. Furthermore, since the inflow boundary layer enhances the heat feedback to the fuel surface to increase mass loss rate, larger fuel dish sizes should be investigated for the same wall heights and enclosure dimensions presented here to change the effective fuel surface area.

Chapter 7: Appendix

For cases where the gap size was the varied quantity, the wall height was fixed at $W = 55cm$. The dimensionless flame length, calculated by Equation 5.2 with the fuel dish diameter as the horizontal length scale, is shown as a function of gap size in Figure 7.1. The nondimensional heat release rate, calculated by Equation 5.1, is shown as a function of the gap size in Figure 7.2 with the flame width as the relevant horizontal length scale. For experiments with varying gap size for a fixed wall height, the dimensionless flame length is shown as a function of the dimensionless heat release rate in Figure 7.3, with both quantites using the flame width as the horizontal length scale.

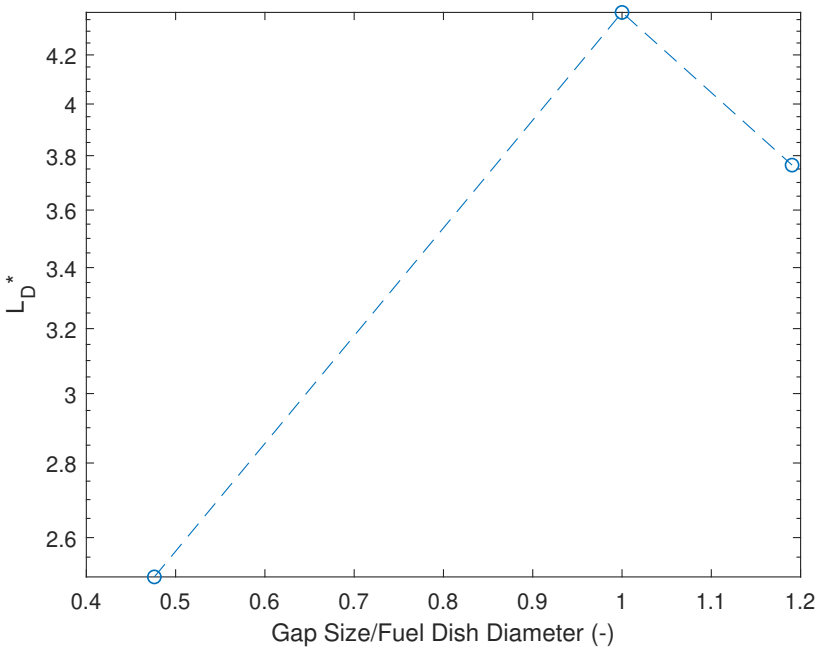

Figure 7.1: Flame length in terms of fuel dish diameters as a function of Gap Size to Fuel Dish Diameter ratio

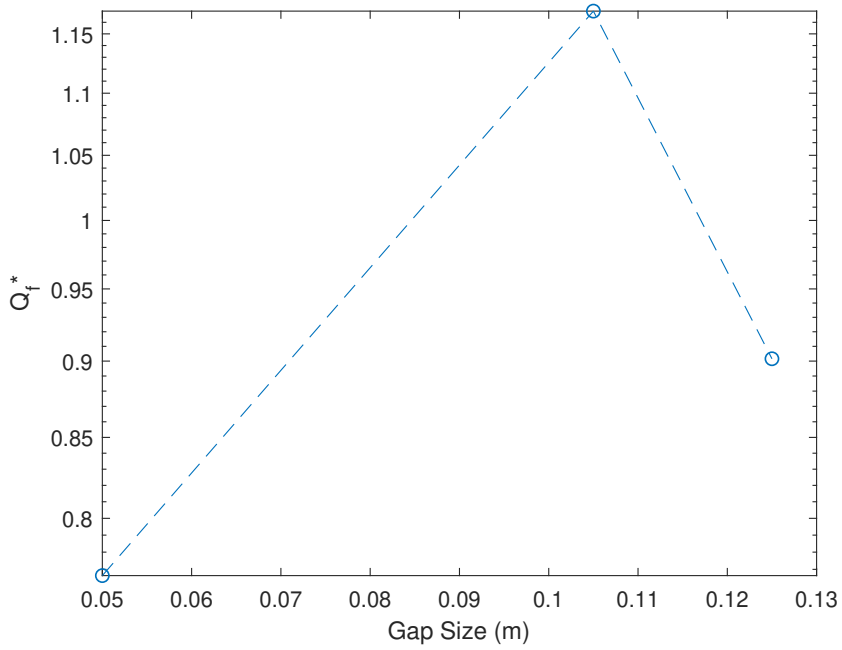

Figure 7.2: Dimensionless Heat Release Rate calculated by Equation 5.1 with flame width as the relevant horizontal length scale as a function of Gap Size for a fixed wall height of 55 cm

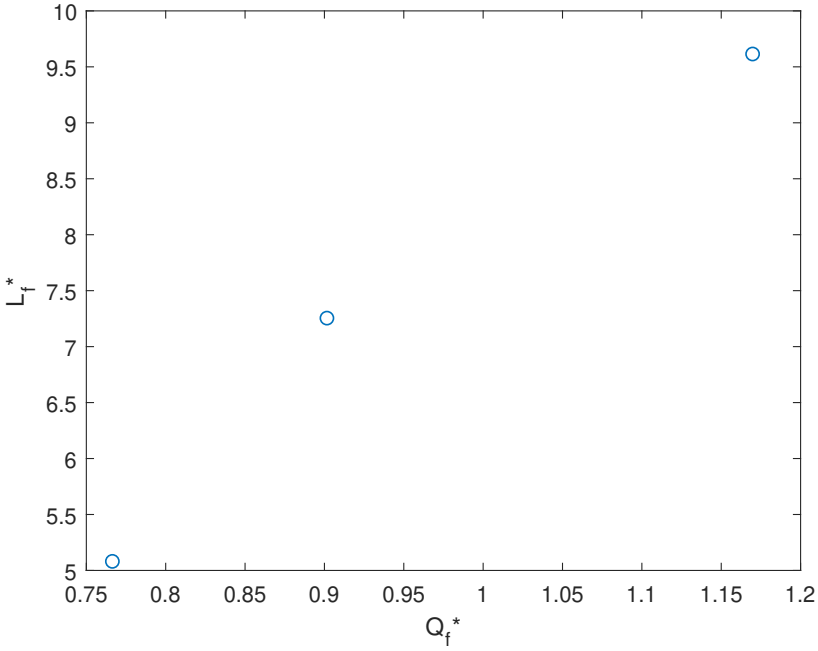

Figure 7.3: Dimensionless Flame length a function of dimensionless Heat Release Rate with the flame width as the relevant horizontal length scale, data shown for tests of varied gap size $G = 5, 10.5, 12.5cm$ but fixed wall height $W = 55cm$

References

[1] G. M. Byram and R. E. Martin, "Fire whirlwinds in the laboratory", *Fire Control Notes*, vol. 23, no. 1, pp. 13–17, 1962.

[2] J. J. Sharples, A. E. Kiss, J. Raposo, D. X. Viegas, and C. C. Simpson, "Pyrogenic vorticity from windward and lee slope fires", *Proceedings - 21st International Congress on Modelling and Simulation, MODSIM 2015*, pp. 291–297, 2015.

[3] K. Kuwana, K. Sekimoto, K. Saito, and F. A. Williams, "Scaling fire whirls", vol. 43, pp. 252–257, 2008. DOI: 10.1016/j.firesaf.2007.10.006.

[4] A. Tohidi, M. J. Gollner, and H. Xiao, "Fire Whirls", *Annual Review of Fluid Mechanics*, vol. 50, no. 1, pp. 187–213, Jan. 2018, ISSN: 0066-4189. DOI: 10.1146/annurev-fluid-122316-045209. [Online]. Available: http://www.annualreviews.org/doi/10.1146/annurev-fluid-122316-045209.

[5] H. Xiao, M. J. Gollner, and E. S. Oran, "From fire whirls to blue whirls and combustion with reduced pollution", vol. 113, no. 34, pp. 9457–9462, 2016. DOI: 10.1073/pnas.1605860113.

[6] M. J. Gollner, E. S. Oran, S. B. Hariharan, J. Dowling, H. F. Farahani, and A. S. Rangwala, "Efficient Remediation of Oil Spills over Water using Fire Whirls (Project Number 1094)", Bureau of Safety and Enivronmental Enforcement, Tech. Rep., 2019. [Online]. Available: https://www.bsee.gov/research-record/efficient-remediation-of-oil-spills-over-water-using-fire-whirls.

[7] L. Buist, J. McCourt, S. Potter, S. Ross, and K. Trudel, "In situ burning", *Pure and Applied Chemistry*, vol. 71, no. 1, pp. 43–65, 1999, ISSN: 00334545. DOI: 10.1351/pac199971010043.

[8] H. W. Emmons and S. J. Ying, "The fire whirl", in *Symposium (International) on Combustion*, vol. 11, 1967, pp. 475–488. DOI: 10.1016/S0082-0784(67)80172-3.

[9] J. Gorman, "New form of fire, inspired by bourbon, might help with oil spills", *New York Times*, Aug. 2016.

[10] J. G. Quintere, *Fundamentals of Fire Phenomena*. John Wiley and Sons, LTD, 2006, ISBN: 978-0-470-09113-5.

[11] A. Y. Snegirev, J. A. Marsden, J. Francis, and G. M. Makhviladze, "Numerical studies and experimental observations of whirling flames", *International Journal of Heat and Mass Transfer*, vol. 47, no. 12-13, pp. 2523–2539, 2004, ISSN: 00179310. DOI: 10.1016/j.ijheatmasstransfer.2004.02.002.

[12] J. Lei, N. Liu, L. Zhang, and K. Satoh, "Temperature, velocity and air entrainment of fire whirl plume: A comprehensive experimental investigation", *Combustion and Flame*, vol. 162, no. 3, pp. 745–758, 2015, ISSN: 15562921. DOI: 10.1016/j.combustflame.2014.08.017. [Online]. Available: http://dx.doi.org/10.1016/j.combustflame.2014.08.017.

[13] S. Li, Q. Yao, and C. K. Law, "The bottom boundary-layer structure of fire whirls", *Proceedings of the Combustion Institute*, vol. 37, no. 3, pp. 4277–4284, 2019, ISSN: 15407489. DOI: 10.1016/j.proci.2018.05.009.

[14] K. A. Hartl, "EXPERIMENTAL INVESTIGATION OF LABORATORY FIRE WHIRLS", PhD thesis, Princeton University, 2016.

[15] J. Lei, N. Liu, L. Zhang, H. Chen, L. Shu, P. Chen, Z. Deng, J. Zhu, K. Satoh, and J. L. De Ris, "Experimental research on combustion dynamics of medium-scale fire whirl", *Proceedings of the Combustion Institute*, vol. 33, no. 2, pp. 2407–2415, 2011, ISSN: 15407489. DOI: 10.1016/j.proci.2010.06.009. [Online]. Available: http://dx.doi.org/10.1016/j.proci.2010.06.009.

[16] M. I. Hassan, K. Kuwana, K. Saito, and F. Wang, "Flow Structure of a Fixed-frame Type Fire Whirl", Tech. Rep., 2005.

[17] P. K. Kundu, I. M. Cohen, and D. R. Dowling, "Chapter 13 - Geophysical Fluid Dynamics", in *Fluid Mechanics (Sixth Edition)*, Academic Press, 2016, ch. 13, pp. 699–771, ISBN: 9781786340276. DOI: 10.1142/9781786340276{_}0001.

[18] R. Yamada and K. Kuwana, "Scaling laws of flow structures around geometrically similar fire whirls", *Journal of Thermal Science and Technology*, vol. 14, no. 1, 2019, ISSN: 18805566. DOI: 10.1299/jtst.2019jtst0009.

[19] K. H. Chuah, K. Kuwana, and K. Saito, "Modeling a fire whirl generated over a 5-cm-diameter methanol pool fire", *Combustion and Flame*, vol. 156, no. 9, pp. 1828–1833, 2009, ISSN: 0010-2180. DOI: 10.1016/j.combustflame.2009.06.010. [Online]. Available: http://dx.doi.org/10.1016/j.combustflame.2009.06.010.

[20] Y. Hayashi, K. Kazunori, and R. Dobashi, "Influence of Vortex Structure on Fire Whirl Behavior", *Fire Safety Science*, vol. 10, pp. 671–679, 2011.

[21] K. H. Chuah and G. Kushida, "The prediction of flame heights and flame shapes of small fire whirls", *Proceedings of the Combustion Institute*, vol. 31 II, pp. 2599–2606, 2007, ISSN: 15407489. DOI: 10.1016/j.proci.2006.07.109.

[22] R. Dobashi, T. Okura, R. Nagaoka, Y. Hayashi, and T. Mogi, "Experimental Study on Flame Height and Radiant Heat of Fire Whirls", *Fire Technology*, vol. 52, no. 4, pp. 1069–1080, Jul. 2016, ISSN: 15728099. DOI: 10.1007/s10694-015-0549-z.

[23] K. Kuwana, S. Morishita, R. Dobashi, K. H. Chuah, and K. Saito, "The burning rate's effect on the flame length of weak fire whirls", *Proceedings of the Combustion Institute*, vol. 33, no. 2, pp. 2425–2432, 2011, ISSN: 15407489. DOI: 10.1016/j.proci.2010.05.049.

[24] J. Lei, N. Liu, L. Zhang, Z. Deng, N. K. Akafuah, T. Li, K. Saito, and K. Satoh, "Burning rates of liquid fuels in fire whirls", *Combustion and Flame*, vol. 159, no. 6, pp. 2104–2114, 2012, ISSN: 15562921. DOI: 10.1016/j.combustflame.2012.01.019. [Online]. Available: http://dx.doi.org/10.1016/j.combustflame.2012.01.019.

[25] S. Burke and T. Schumann, "Diffusion Flames", in *Proceedings of the Symposium on Combustion*, 1948, pp. 2–11. DOI: 10.1016/b978-012285852-9/50007-2.

[26] H. Tennekes and J. L. Lumley, "The Dynamics of Turbulence", in *A First Course in Turbulence*, Cambirdge, Massachusetts: The MIT Press, 1972, ch. 3, pp. 59–103.

[27] W. Coenen, E. J. Kolb, A. L. Sánchez, and F. A. Williams, "Observed dependence of characteristics of liquid-pool fires on swirl magnitude", *Combustion and Flame*, vol. 205, pp. 1–6, Jul. 2019, ISSN: 15562921. DOI: 10.1016/j.combustflame.2019.03.032.

[28] J. Lei, N. Liu, Y. Jiao, and S. Zhang, "Experimental investigation on flame patterns of buoyant diffusion flame in a large range of imposed circulations", *Proceedings of the Combustion Institute*, vol. 36, no. 2, pp. 3149–3156, 2017, ISSN: 15407489. DOI: 10.1016/j.proci.2016.06.072. [Online]. Available: http://dx.doi.org/10.1016/j.proci.2016.06.072.

[29] Y. Hu, S. B. Hariharan, H. Qi, M. J. Gollner, and E. S. Oran, "Conditions for formation of the blue whirl", *Combustion and Flame*, vol. 205, pp. 147–153, 2019, ISSN: 15562921. DOI: 10.1016/j.combustflame.2019.03.043.

[30] K. A. Hartl and A. J. Smits, "Scaling of a small scale burner fire whirl", *Combustion and Flame*, vol. 163, pp. 202–208, 2016, ISSN: 15562921. DOI: 10.1016/j.combustflame.2015.09.027.

[31] K. Satoh and K. Yang, "Simulations Of Swirling Fires Controlled By Channeled Self-generated Entrainment Flows", *Fire Safety Science*, vol. 5, pp. 201–212, 1997, ISSN: 18174299. DOI: 10.3801/iafss.fss.5-201.

[32] J. G. Q. Bjorn Karlsson, *Enclosure Fire Dynamics*, A. K. Gupta and D. G. Lilley, Eds. CRC Press, 2000, ISBN: 0-8493-1300-7.

[33] J. Lei, N. Liu, and K. Satoh, "Buoyant pool fires under imposed circulations before the formation of fire whirls", *Proceedings of the Combustion Institute*, vol. 35, no. 3, pp. 2503–2510, 2015, ISSN: 15407489. DOI: 10.1016/j.proci.2014.05.110. [Online]. Available: http://dx.doi.org/10.1016/j.proci.2014.05.110.

[34] K. Zhou, N. Liu, J. S. Lozano, Y. Shan, B. Yao, and K. Satoh, "Effect of flow circulation on combustion dynamics of fire whirl", *Proceedings of the Combustion Institute*, vol. 34, no. 2, pp. 2617–2624, 2013, ISSN: 15407489. DOI: 10.1016/j.proci.2012.06.053.